Technical Report

TR-99-26

Experimental determination and chemical modelling of radiolytic processes at the spent fuel/water interface

Jordi Bruno, Esther Cera, Mireia Grivé
QuantiSci SL, Barcelona

Ulla-Britt Eklund
Studsvik Nuclear AB, Nyköping

Trygve Eriksen
Department Nuclear Chemistry
Kungliga Tekniska Högskolan, Stockholm

November 1999

Svensk Kärnbränslehantering AB
Swedish Nuclear Fuel
and Waste Management Co
Box 5864
SE-102 40 Stockholm Sweden
Tel 08-459 84 00
+46 8 459 84 00
Fax 08-661 57 19
+46 8 661 57 19

Experimental determination and chemical modelling of radiolytic processes at the spent fuel/water interface

Jordi Bruno, Esther Cera, Mireia Grivé
QuantiSci SL, Barcelona

Ulla-Britt Eklund
Studsvik Nuclear AB, Nyköping

Trygve Eriksen
Department Nuclear Chemistry
Kungliga Tekniska Högskolan, Stockholm

November 1999

Keywords: radionuclides, radiolysis products, spent fuel, thermodynamic

Abstract

The spent fuel matrix in contact with water constitutes a dynamic redox system due to the time dependent radiolytic generation of oxidants and reductants at the fuel interface. In this context it is important to understand the main processes and mechanisms that control the impact of radiolytically generatet reactants on the stability of the UO_2-matrix and release of radionuclides.

A series of carefully controlled time resolved experiments have been carried out in order to determine the radiolytical generation of hydrogen, hydrogen peroxide and oxygen and the release of radionuclides in an initially anoxic system containing fuel fragments in contact with distilled water and Na HCO_3 solutions.

The experimental data, being quite reproducible and consistent, indicate that it is possible to define a bulk redox potential for the main redox pairs in the solution and that the experimentally determined radionuclide concentrations can be rationalised in terms of this potential. Mass balance calculations indicate that consumption of radiolytically produced oxidants by the fuel corresponds to the formation of an oxidised UO_{2+x} surface layer in distilled water and the formation and release of soluble U(VI)- carbonate complexes in bicarbonate media.

Uranium release at early contact times is controlled by oxidative dissolution of the fuel matrix. This process also controls the release of Sr, Np and Pu. The measured concentrations of the actinides appear to be limited by the solubility of Ac(IV) hydroxide phases. The release of Tc and Mo appears to be controlled by oxidative dissolution of their metallic phases, Mo showing higher oxygen affinity than Tc in accordance with their thermodynamic properties. The behaviour of the lanthanides Nd and Y gives no evidence of congruent release with the fuel matrix. Cs is preferentially dissolved in agreement with earlier observations.

Long time experiments indicate that some elements reach saturation with respect to secondary phases. Uranium concentrations seem to be in equilibrium with U(VI)-oxyhydroxide in all experiments with exception of experiments carried out with the highest bicarbonate concentration (10 mM) as the stability of the U(VI)-carbonate complexes hinders precipitation of other secondary phases.

Np and Pu seem to be solubility limited by the formation of their Ac(IV) hydroxide phases and Tc by the formation of a Tc(IV) hydroxide phase. Sr is not close to saturation with respect to any secondary phase, thereby confirming its role as a matrix dissolution marker.

Sammanfattning

Bestrålat kärnbränsle i kontakt med vatten utgör ett dynamiskt redoxpar genom den tidsberoende radiolytiska bildningen av oxiderande och reducerande species. För att kunna förutsäga upplösningshastigheten för utbränt bränsle är det viktigt att förstå mekanismerna för oxidation och upplösning av bränslegittret.

I en serie tidsupplösta försök har vi därför mätt bildningen av de långlivade radiolysprodukterna H_2, H_2O_2 och H_2 och utlösningen av radionuklider i ett slutet, initialt anoxiskt system innehållande bränslefragment i kontakt med destillerat vatten eller karbonatlösningar.

Reproducerbara och konsistenta försöksdata indikerar att det är möjligt att definiera en jämviktspotential för de dominerande redoxparen i lösningen och förklara radionuklidernas koncentration med denna potential. Massbalansberäkningar visar att förbrukningen av oxidanter i reaktioner med bränsleytan i destillerat vatten motsvaras av bildningen av ett oxiderat UO_{2+x}-skikt och i karbonatlösningar av bildning av lösliga U(VI)-karbonat komplex.

Utlösning av uran kontrolleras vid korta tider av oxidativ upplösning av bränslegittret. Denna process kontrollerar även utlösningen av Sr, Np och Pu. Mätta aktinidkoncentrationer är sannolikt begränsade av lösligheterna för Ac(IV)-hydroxider. Utlösningen av Tc och Mo indikerar oxidativ upplösning av metalliska faser. Oxidantaffiniteten är, som förväntat från termodynamiska data, större för Mo än för Tc. Cs utlöses preferentiellt i enlighet med tidigare observationer.

Data från långtidsförsök visar att några grundämnen nått mättnad med avseende på bildning av sekundära faser. Urankoncentrationerna motsvarar lösligheten av U(VI)-oxohydroxid i samtliga försök med undantag för försök med hög karbonathalt (10 mM) där U(VI)-karbonatens stabilitet hindrar utfällning av sekundära faser.

Np, Pu och Tc data visar på löslighetsbegränsning genom bildning av Ac(IV) och Tc(IV) hydroxidfaser. Sr(II) är icke nära löslighetsbegränsning av sekundära faser och bekräftar dess roll som matrisupplösningsämne.

Table of contents

1 Introduction

The chemical stability of a repository is defined by its resistance to radionuclide release to the biosphere. This resistance is primarily dependent on the chemical stability of the spent fuel matrix itself and spent fuel is disposed under chemical conditions that guarantee this stability. These chemical conditions are designed and engineered in order to minimise the potential release of radionuclides and are normally described by two intensive parameters (pH and Eh). It is clear that the redox potential is the most critical one to define the stability of the spent fuel matrix. In this context, it is now well established that the confinement of radionuclides within the matrix is guaranteed if the oxidation state of the UO_2 matrix does not exceed the upper limit of stability of the cubic structure, $UO_{2.33}$, which corresponds to a nominal stoichiometry of U_3O_7.

However, the spent fuel matrix constitutes a dynamic redox system by itself. This is because there is a time-dependent generation of oxidants and reductants at the fuel/water interface due to α, β and γ radiolysis. Under these circumstances, it is problematic to treat the spent fuel/water system as a redox equilibrium and consequently the definition of Eh (or pe) as an intensive parameter becomes questionable. The complexity is further increased if we try to integrate additional redox-sensitive components, like the canister or the pyrite content of the bentonite material, into the system under study.

The role of mineral surfaces in poising the redox state of a solid/water system is a well established phenomenon evolving from the concepts developed for heterogeneous electron transfer /White and Yee, 1985/. The fact that the UO_2 spent fuel matrix constitutes a semiconductor would indicate that the basic premises for heterogeneous electron transfer reactions are fulfilled. In the repository situation where the Mass to Volume ratio is particularly high, the UO_2 surface is going to play a key role in defining the redox capacities of the system and consequently its redox state.

Experimental evidence on the role of the UO_2 surfaces both as a reductant and on its redox buffering capacity is now available. In a pioneering work, Eriksen et al /1995/, reported on well controlled experiments aimed at obtaining the mass balance of radiolytically produced oxidants and reductants by spent fuel in contact with distilled water. In these experiments, performed in a closed system, a clear oxidant deficit was observed. The authors explained this oxidant deficit by the effect of their uptake by the UO_2 spent fuel surface. Natural uraninite deposits have also brought clear indications of the redox buffering capacity of the UO_2 surface. Redox measurements performed in groundwaters in contact with the uraninite deposits in Cigar Lake (Canada) /Casas and Bruno, 1994/ and Palmottu (Finland) /Bruno et al, 1996/, indicate that the redox potential could be controlled by the UO_2/U_3O_7 transition.

A kinetic model for the stability of the spent fuel matrix under oxic conditions has been developed under the name of RDC (ReDuctive Capacity) Model /Bruno et al, 1998/, which integrates a mass balance approach with the kinetics of heterogeneous electron transfer and dissolution/precipitation kinetics. The model has proven to reproduce quite satisfactorily experimental data on spent fuel and UO_2 dissolution.

Further development of this work requires to ascertain which is the role of the main groundwater ligands in the generation of radiolytic products and its consequence for radionuclide release.

In order to do this SKB commissioned a series of carefully controlled experiments in order to determine the time dependence of the radiolytic gas production (H_2, O_2 and H_2O_2) and radionuclide release (U, Pu, Np, Y, Nd, Tc, Mo, Sr and Cs) in an anoxic closed system, when PWR Ringhals spent fuel fragments are put in contact with 10 mM $NaHCO_3$ solutions.

The objective of this report is to present the experimental data from these experiments together with the chemical modelling performed in order to rationalise the experimental observations within the conceptual framework of the RDC approach.

2 Experimental

2.1 Material

Various fragments from a PWR fuel rod, Ringhals DO-7-S14 were used in the experiments. The Ringhals DO-7-S14 fuel rod was irradiated for five cycles during 1977-1983 with an average linear power of 18 kW/m. The average calculated burnup is 40 MWd/kgU. Radiation characteristics are given in Table 2-1. The weight of the fragments used in each experiment was approximately 2 g. Test solutions were prepared from Millie-Q purified water purged with AGA 5.7 quality argon, containing less than 0.5 ppm oxygen.

Table 2-1. Inventory of PWR reference fuel 91.10.01.

Energy of α-emitter (MeV)	Activity ($Bq \cdot g^{-1}$)
5.15	$2.86 \cdot 10^{7}$
5.50	$2.00 \cdot 10^{8}$
5.81	$1.15 \cdot 10^{8}$
Major β-emitting nuclides	**Activity ($Bq \cdot g^{-1}$)**
^{241}Pu	$3.00 \cdot 10^{9}$
^{90}Sr	$2.63 \cdot 10^{9}$
$1^{06}Rh$	$4.17 \cdot 10^{7}$
^{125}Sb	$2.53 \cdot 10^{9}$
^{134}Cs	$3.29 \cdot 10^{8}$
^{137}Cs	$3.44 \cdot 10^{9}$
^{144}Ce	$1.41 \cdot 10^{7}$
^{133}Pr	$1.41 \cdot 10^{7}$
^{154}Eu	$1.54 \cdot 10^{8}$
^{155}Eu	$1.53 \cdot 10^{8}$

2.2 Time-resolved experiments

The experimental set up is depicted in Figure 2-1 Fuel fragments were transferred to a quartz vessel with approximately 60 cm^3 total volume. The vessel, containing the fuel fragments, was placed in a lead shield into a glove box with argon atmosphere and connected to gas and solution sampling and analysing systems.

The test dissolution vessel and sensor chamber were flushed with argon through a thin plastic tube inserted into the vessel via the sensor chamber. A volume of 30 cm^3 solution containing 10 mM bicarbonate was transferred through the same plastic tube to the vessel by applying argon overpressure to a stock solution reservoir. The tube was thereafter removed and the valve connecting the reaction vessel and sensor chamber closed.

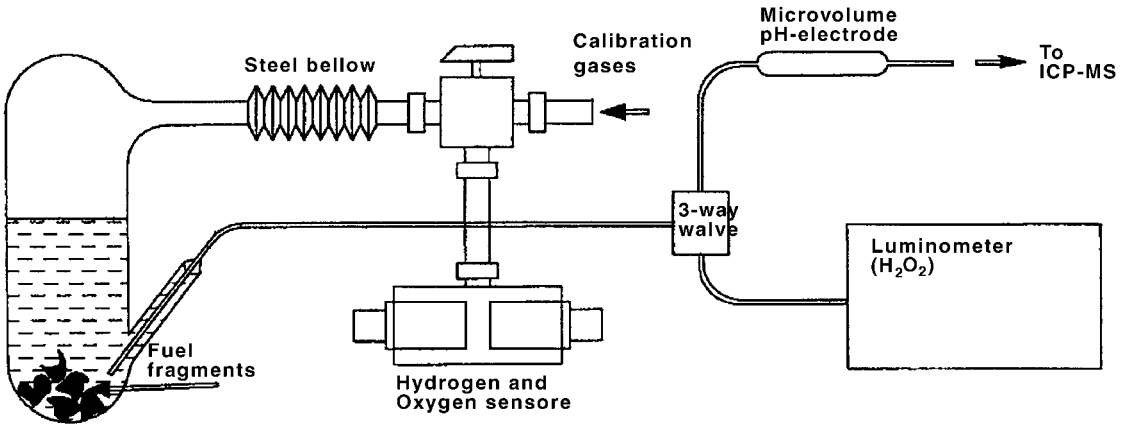

Figure 2-1. *Experimental set up.*

2.2.1 Gas analysis

The oxygen and hydrogen gas detector system (Orbisphere 3600/111E, 31130 O_2 and 3600/2111E 31230 H_2 detectors) was calibrated by flushing the sensor chamber with standardised gas mixtures. After calibration the sensor chamber was flushed with argon, and the inlet and outlet valves closed. The reaction vessel/sensor chamber valve was opened thereafter allowing the radiolytically formed oxygen and hydrogen to diffuse into the sensor chamber. Detector readings were taken at time intervals to minimise oxygen and hydrogen consumption by the detectors.

2.2.2 Solution analysis

Small volumes (1–2 cm^3) of the test solution were at time intervals removed through a capillary tube for analysis.

Hydrogen peroxide was measured by means of a luminescence method earlier described in detail by Eriksen et al /1995/.

Fission products were analysed with ICP-MS (Plasma Quad 2 Plus, VG Elemental UK). The analytical samples were prepared with a 1 ppb internal ^{115}In reference standard. Mass peak counts over the whole range (82 to 254) are related to the ^{115}In signal, yielding a series of ratios. Sensitivity factors relative to ^{115}In were determined using a range of natural multielement standards and radionuclide standards for Tc-99 and Pu.

Uranium was monitored by mass/charge 119 (U^{2+}) and mass 254 (UO^+). Plutonium was monitored by mass 240 in order to avoid uranium interference for the isotope with mass 239. Pu-240 is taken to be 30% of total plutonium according the inventory. Fission produced strontium was monitored by Sr-90 and corrected by assuming the composition in the inventory to be 60% Sr-90 and 40% Sr-88. The uranium concentration was also measured using laser fluorimetry (Scintrex UA-3).

2.3 Long contact time experiments

The ampoules to be used in the long time experiments, loaded with approximately 2 g fuel fragments, were placed in a lead shield in a glove box with argon atmosphere. The ampoules were flushed with argon, 14 cm^3 solution was transferred to each ampoule and the ampoules sealed using a gas burner. The ampoules were stored in air for 396 to 470 days.

At the end of the experiment the ampoules were moved to the glove box with argon atmosphere, and connected to the gas analysing system. The analysing system was flushed with argon; the thin ampoule membrane broken and the gas phase analysed for oxygen and hydrogen as described above.

Following the gas analysis, the solution samples were analysed for hydrogen peroxide, uranium and fission products.

Distilled water, 2 and 10 mM bicarbonate solutions and artificial ground water (Allard solution) were used as test solutions.

3 Radiolysis

The solution surrounding the fuel fragments is exposed to a field of mixed radiation, α, β in an approximately 40 μm thick layer closest to the fragment surface, β,γ in the bulk solution.

Equivalent amounts of oxidising and reducing species are formed by radiolysis of water, the total and relative yields being radiation type dependent.

The yields of primary species formed on radiolysis of water by α and β radiation are given in Table 3-1.

In solutions secondary oxidising and reducing species are formed in reactions with the primary ones, e.g. in carbonate solutions the oxidant CO_3^- is formed by OH· oxidation of the carbonate/bicarbonate anion.

Table 3-1. Yields of primary products (mole dm^{-3} x 10^7) formed on radiolysis of water.

Species	β	α
H_2O	-4.30	-2.87
H_2	0.45	1.30
H_2O_2	0.75	0.985
e^-_{aq}	2.80	0.06
H·	0.60	0.21
·OH	2.80	0.24
H^+	2.80	0.06
HO_2·	–	0.22

4 Results

4.1 Time-resolved experiments

4.1.1 Radiolysis products

The experimental data on the oxidants and reductants generated by the radiolysis of the water are given in the appendix (Table 8-1).

The following graphs show the concentration of these species in solution as a function of the contact time for each experiment.

The concentration of oxygen and hydrogen in solution has been calculated according to the following equation:

$$[X] = ppm \times 10^{-6} \times K_H^{\ x} \qquad (4\text{-}1)$$

where ppm denotes the concentration of either oxygen or hydrogen in the gas phase expressed in ppm in volume and $K_h^{\ x}$ stands for the Henry's law constant at 1 bar and 25 ^{o}C. K_H is equal to $1.26 \cdot 10^{-3}$ mole·dm^{-3} for oxygen and $8.11 \cdot 10^{-4}$ mole·dm^{-3} for hydrogen /Stumm and Morgan, 1981/.

As we can see in Figures 4-1 to 4-4, the concentration of oxygen and hydrogen as a function of time follow the same trend in all the tests. However, in the first run the concentrations of both compounds are at similar levels (Figure 4-1) while in the following experiments, the hydrogen concentration in solution is larger than the oxygen concentration, as can be observed in Figures 4-2 to 4-4.

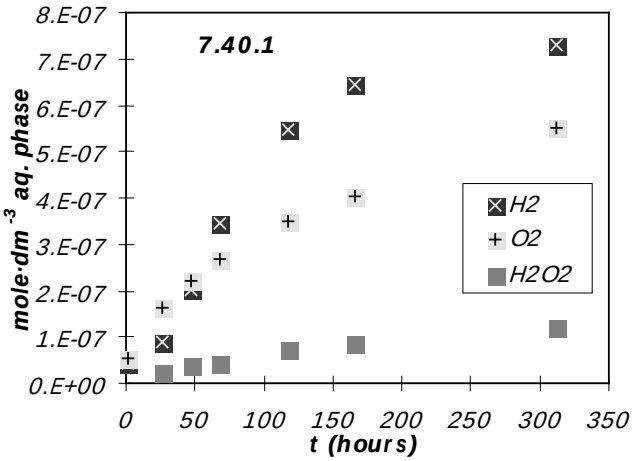

Figure 4-1. *Hydrogen, hydrogen peroxide and oxygen concentrations in solution as a function of time. Test 7.40.1.*

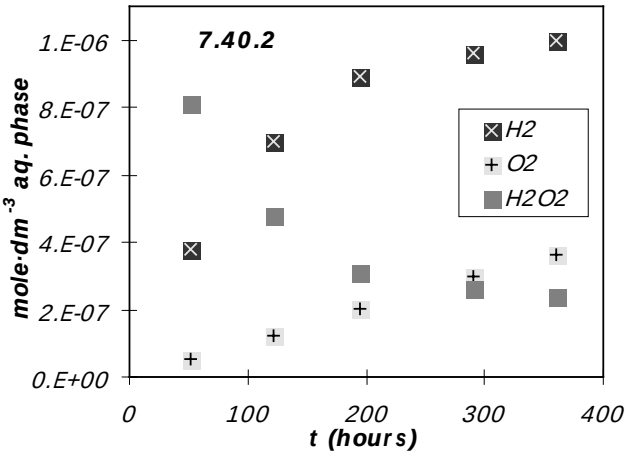

Figure 4-2. *Hydrogen, hydrogen peroxide and oxygen concentrations in solution as a function of time. Test 7.40.2.*

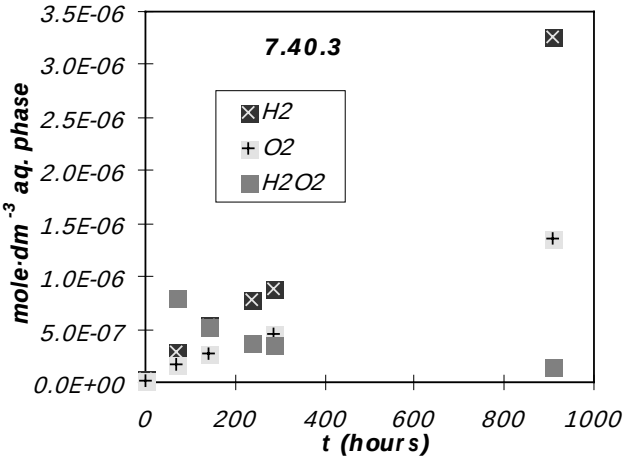

Figure 4-3. *Hydrogen, hydrogen peroxide and oxygen concentrations in solution as a function of time. Test 7.40.3.*

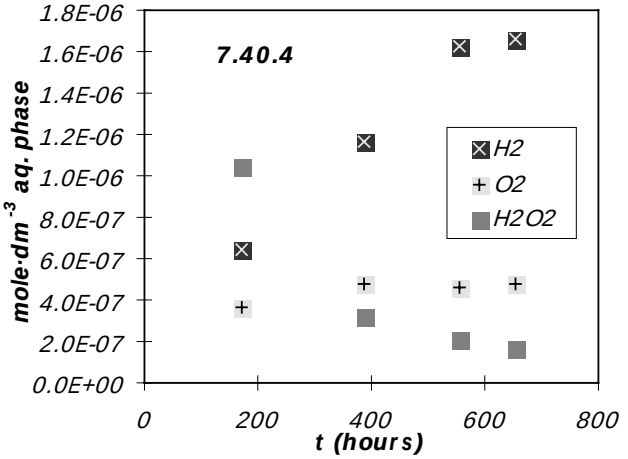

Figure 4-4. *Hydrogen, hydrogen peroxide and oxygen concentrations in solution as a function of time. Test 7.40.4.*

The hydrogen peroxide concentration as a function of time shows a variable behaviour depending on the run. In the first run (Figure 4-1), the concentration of hydrogen peroxide increases with time, but is always lower than the oxygen and the hydrogen concentrations. On the contrary, in the successive experiments, the concentration of hydrogen peroxide decreases with contact time. At short contact times, the concentration of hydrogen peroxide is larger than the measured concentrations of hydrogen and oxygen. At longer contact times, and due to the consumption of hydrogen peroxide, dissolved oxygen and hydrogen concentrations are at higher levels (Figures 4-2 to 4-4).

4.1.2 Radionuclide concentrations in solution

The solution concentrations of the different radionuclides measured at different time intervals are given in Table 8-2 in the appendix. The time evolution of the radionuclide concentration is also presented in the following graphs (Figures 4-5 to 4-9).

The concentration of uranium in solution increases with time in all the experiments (Figure 4-5). The uranium concentration in the first run is at all times higher than the concentration measured in the successive tests showing the different nature of the contacting surface. The fact that this initial release is consistently measured for all redox dependent nuclides and with particular emphasis in the case of uranium indicates that this is due to the dissolution of a partly oxidised surface layer of the spent fuel sample.

Neptunium concentrations in solution follow the same trend as uranium; the concentration increases in solution with time in each experimental test (Figure 4-6). However, the differences in the concentration measured in each run were smaller than in the case of uranium. Plutonium follows the same trend as uranium only in the first experiment. In the successive runs plutonium behaves in a completely different manner with respect to uranium. After an initial sharp increase, the concentration of plutonium decreases with time to reach a steady state value. This would indicate that, after the initial dissolution of the oxidised surface layer, precipitation of a secondary Pu solid phase controls its behaviour in experiments 7.40.2 to 7.40.4. (Figure 4-6).

The evolution of strontium and caesium concentrations with time shows the same trend as for uranium (Figure 4-7). Again, the measured strontium concentrations in the first run were higher than in the other three showing the same pattern as uranium. This parallelism could indicate a co-dissolution process of strontium with uranium, the major component of the fuel sample. The release of caesium is larger in the first experiment 7.40.1, and decreases in the following experiments, which is in agreement with the increased concentration of this radionuclide at the fuel surface.

Molybdenum and technetium concentrations with time show the same behaviour as uranium (Figure 4-8). The similarity in their behaviour could also indicate a co-dissolution process with the major component of the system governing the release of these radionuclides from the fuel.

Finally, the evolution of yttrium and neodymium concentrations with contact time is completely different to the evolution of the major component of the fuel (Figure 4-9). This different behaviour could indicate that these lanthanides are solubility controlled after the initial higher release from the oxidised surface in experiment 7.40.1.

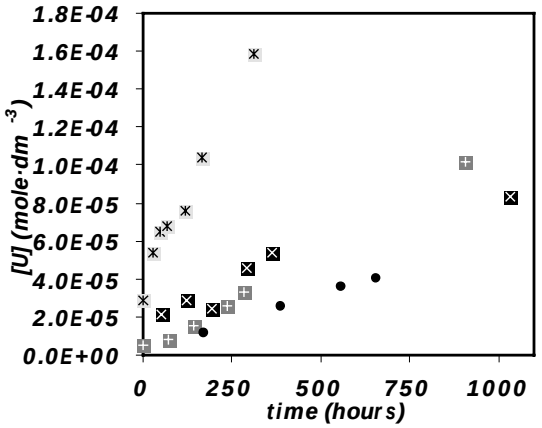

Figure 4-5. *Evolution of the uranium concentration with time. 7.40.1:light grey dots; 7.40.2:black dots; 7.40.3:dark grey dots; 7.40.4:black circles.*

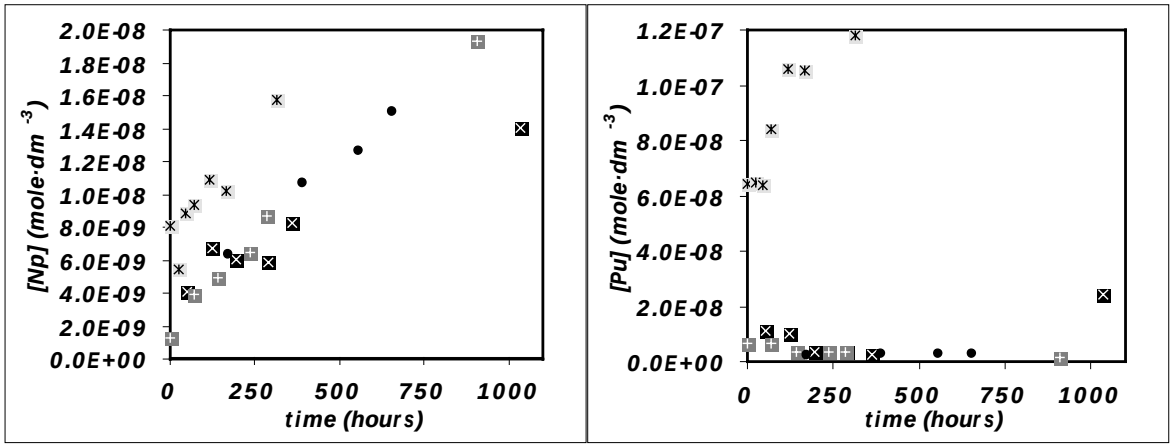

Figure 4-6. *Evolution of the neptunium (left) and plutonium (right) concentrations with time. 7.40.1:light grey dots; 7.40.2:black dots; 7.40.3:dark grey dots; 7.40.4:black circles.*

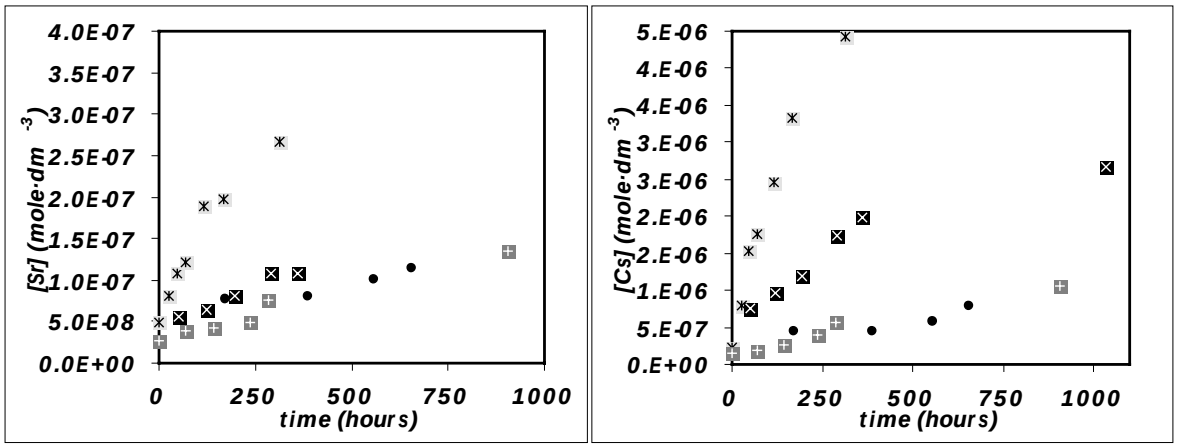

Figure 4-7. *Evolution of the strontium (left) and caesium (right) concentrations with time. 7.40.1: light grey dots; 7.40.2: black dots; 7.40.3:dark grey dots; 7.40.4: black circles.*

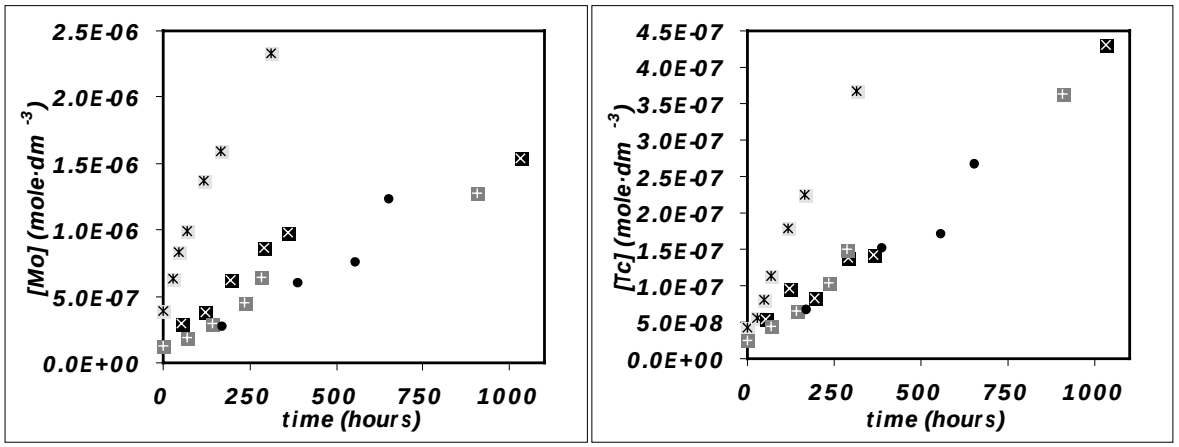

Figure 4-8. *Evolution of the molybdenum (left) and technetium (right) concentrations with time. 7.40.1: light grey dots; 7.40.2: black dots; 7.40.3: dark grey dots; 7.40.4: black circles.*

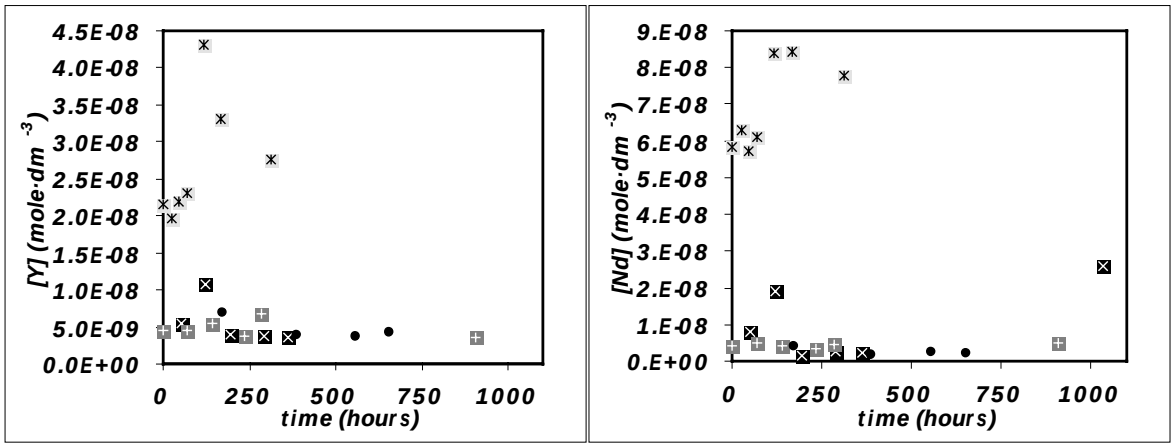

Figure 4-9. *Evolution of the yttrium (left) and neodymium (right) concentrations with time. 7.40.1: light grey dots; 7.40.2: black dots; 7.40.3: dark grey dots; 7.40.4: black circles.*

4.2 Long time experiments

The primary data concerning the oxidants and reductants generated by the radiolysis of the water as well as the concentration of the different elements measured at the end of the experiments are given in the appendix (Table 8-3).

Four solutions were used in these experiments and each experiment was carried out twice, using different fuel fragments in order to obtain duplicates of the data. The graphs in Figure 4-10 show the results obtained for the duplicates in the four sets of experiments for some of the compounds measured in gaseous or in aqueous phase.

As can be observed in the graphs there are important differences in the measured data taking into account that duplicates were performed under the same experimental conditions although the experimental time was slightly different. In the duplicated experiments (second columns in the figures for each set of experiments) the fuel fragments remained in contact with the solution for a longer time than the first ones. However, the different behaviour observed depending on both the compound and the

solution used is an indication of the variability and complexity of the systems studied in these experiments.

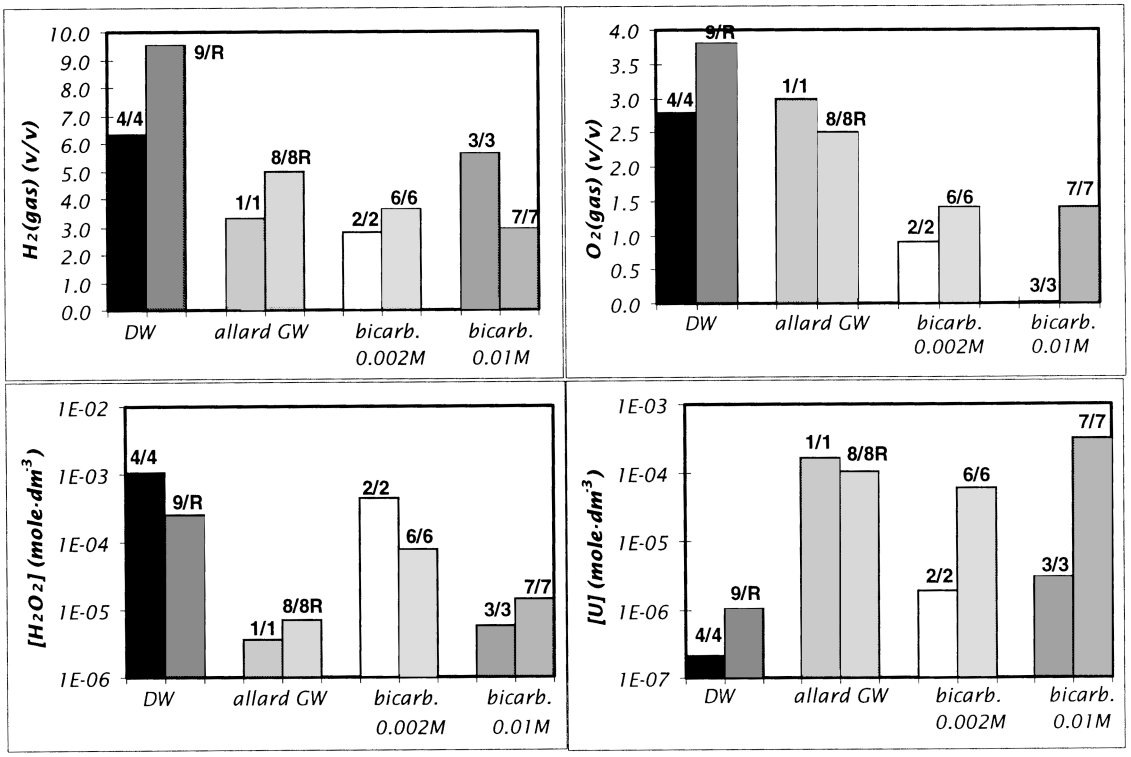

Figure 4-10. *Hydrogen and oxygen contents measured in the gas phase and hydrogen peroxide and uranium concentrations measured in solution in each experiment.*

5 Discussion

5.1 Time-resolved experiments

5.1.1 Radiolysis products

The overall production of oxidants and reductants in each test is reflected in the electron balance calculated by using the experimental data concerning the observed concentrations of the major oxidising and reducing species (Table 5-1).

In the column Red-Ox of Table 5-1, we have calculated the electron balance by considering the hydrogen, oxygen and hydrogen peroxide concentrations measured in the gas and aqueous phases according to the following equation:

$$2 \times [H_2] - 4 \times [O_2] - 2 \times [H_2O_2] \qquad (5\text{-}1)$$

As we can see, initially there is an excess of radiolytically formed oxidants with respect to reductants in experiment 7.40.1, due to the higher generation of oxygen than hydrogen at short contact times (under 50 hours), see Figure 4-1. At longer contact times, the trend changes and the net balance gives a larger concentration of reductants than oxidants in the system. On the other hand, in experiments 7.40.2, 7.40.3 and 7.40.4, there is in general an excess of hydrogen in the system with respect the oxidants generated as we can see in the same table.

If we include in the electron balance calculations the contribution from the dissolved uranium, assuming that all the measured uranium is hexavalent, the uranium released from the fuel matrix as a consequence of the oxidation of UO_2 (eq. 5-2), the situation changes.

$$2 \times [H_2] - 4 \times [O_2] - 2 \times [H_2O_2] - 2 \times [U(VI)] \qquad (5\text{-}2)$$

The results indicate in general a nominal electron balance of the system with the exception of experiment 7.40.1. The fuel fragments used in this experiment were not pretreated to clean the surfaces. Consequently, the surfaces were most probably partly oxidised. The net oxidant consumption for each dissolved U(VI) will therefore initially be lower.

As we can see in Table 5-1, the excess of reductants from the electron balance when considering only the water radiolysis products is compensated by uranium released to the aqueous phase, giving a net balance which in most cases is close to zero (within the analytical uncertainty). This behaviour is clearly different from the one obtained in the previous radiolytic mass balance experiments performed in deionised water /Eriksen et al, 1995/, where the electron unbalance observed in the solutions used in these experiments was attributed to the oxidant uptake by the UO_2 surface to form UO_{2+x}. The present experiments have been carried out in 10^{-2} mole·dm^{-3} bicarbonate solution, thus the high stability of the U(VI)-carbonate aqueous complexes favours the release of the uranium from the UO_2 matrix and consequently the formation of an oxidised surface layer is not expected. In both cases, the oxidation of U(IV) to U(VI), either in the solid surface or in the solution is the process responsible for compensating the redox unbalance caused by the radiolytic reactions at the spent fuel/water interface.

Table 5-1. Electron balance calculated by using the experimental data.

	$molO_2(g)$	$molO_2(aq)$	$molH_2(g)$	$molH_2(aq)$	$molH_2O_2$	Red-Ox (eq.)	U(VI) (eq.)	Red-Ox-U(VI) (eq.)	mean value +σ
7:40:1:I	$5.76\cdot10^{-8}$	$1.63\cdot10^{-9}$	$7.10\cdot10^{-8}$	$1.29\cdot10^{-9}$			$1.73\cdot10^{-6}$		
7:40:1:II	$1.76\cdot10^{-7}$	$4.72\cdot10^{-9}$	$1.51\cdot10^{-7}$	$2.61\cdot10^{-9}$	$7.31\cdot10^{-10}$	$-4.16\cdot10^{-7}$	$3.13\cdot10^{-6}$	$-3.55\cdot10^{-6}$	
7:40:1:III	$2.58\cdot10^{-7}$	$6.02\cdot10^{-9}$	$3.64\cdot10^{-7}$	$5.46\cdot10^{-9}$	$1.03\cdot10^{-9}$	$-3.20\cdot10^{-7}$	$3.51\cdot10^{-6}$	$-3.83\cdot10^{-6}$	
7:40:1:IV	$3.36\cdot10^{-7}$	$6.71\cdot10^{-9}$	$6.68\cdot10^{-7}$	$8.59\cdot10^{-9}$	$1.07\cdot10^{-9}$	$-1.81\cdot10^{-8}$	$3.38\cdot10^{-6}$	$-3.39\cdot10^{-6}$	
7:40:1:V	$4.54\cdot10^{-7}$	$8.05\cdot10^{-9}$	1.11E-06	$1.27\cdot10^{-8}$	$1.69\cdot10^{-9}$	$3.91\cdot10^{-7}$	$3.53\cdot10^{-6}$	$-3.14\cdot10^{-6}$	
7:40:1:VI	$5.64\cdot10^{-7}$	$8.43\cdot10^{-9}$	1.40E-06	$1.34\cdot10^{-8}$	$1.77\cdot10^{-9}$	$5.25\cdot10^{-7}$	$4.34\cdot10^{-6}$	$-3.81\cdot10^{-6}$	
7:40:1:VII	$8.15\cdot10^{-7}$	$1.02\cdot10^{-8}$	1.67E-06	$1.34\cdot10^{-8}$	$2.21\cdot10^{-9}$	$5.58\cdot10^{-8}$	$5.84\cdot10^{-6}$	$-5.79\cdot10^{-6}$	
									$-3.92\cdot10^{-6}\pm 8.69\cdot10^{-7}$
7:40:2:I	$5.89\cdot10^{-8}$	$1.66\cdot10^{-9}$	$6.24\cdot10^{-7}$	$1.13\cdot10^{-8}$	$2.43\cdot10^{-8}$	$9.80\cdot10^{-7}$	$1.29\cdot10^{-6}$	$-3.06\cdot10^{-7}$	
7:40:2:II	$1.36\cdot10^{-7}$	$3.42\cdot10^{-9}$	$1.25\cdot10^{-6}$	$1.98\cdot10^{-8}$	$1.36\cdot10^{-8}$	$1.94\cdot10^{-6}$	$1.65\cdot10^{-6}$	$2.94\cdot10^{-7}$	
7:40:2:III	$2.47\cdot10^{-7}$	$5.36\cdot10^{-9}$	$1.70\cdot10^{-6}$	$2.37\cdot10^{-8}$	$8.24\cdot10^{-9}$	$2.42\cdot10^{-6}$	$1.31\cdot10^{-6}$	$1.11\cdot10^{-6}$	
7:40:2:IV	$3.92\cdot10^{-7}$	$7.22\cdot10^{-9}$	$1.97\cdot10^{-6}$	$2.33\cdot10^{-8}$	$6.31\cdot10^{-9}$	$2.38\cdot10^{-6}$	$2.21\cdot10^{-6}$	$1.68\cdot10^{-7}$	
7:40:2:V	$5.05\cdot10^{-7}$	$8.28\cdot10^{-9}$	$2.17\cdot10^{-6}$	$2.29\cdot10^{-8}$	$5.50\cdot10^{-9}$	$2.32\cdot10^{-6}$	$2.46\cdot10^{-6}$	$-1.42\cdot10^{-7}$	
									$2.26\cdot10^{-7}\pm 4.93\cdot10^{-7}$
7:40:3:I	$2.01\cdot10^{-8}$	$5.67\cdot10^{-10}$	$6.03\cdot10^{-8}$	$1.09\cdot10^{-9}$		$4.01\cdot10^{-8}$	$3.27\cdot10^{-7}$		
7:40:3:II	$1.88\cdot10^{-7}$	$4.74\cdot10^{-9}$	$5.10\cdot10^{-7}$	$8.25\cdot10^{-9}$	$2.26\cdot10^{-8}$	$2.19\cdot10^{-7}$	$4.60\cdot10^{-7}$	$-2.41\cdot10^{-7}$	
7:40:3:III	$3.28\cdot10^{-7}$	$6.93\cdot10^{-9}$	$1.02\cdot10^{-6}$	$1.39\cdot10^{-8}$	$1.36\cdot10^{-8}$	$7.08\cdot10^{-7}$	$7.79\cdot10^{-7}$	$-7.06\cdot10^{-8}$	
7:40:3:IV	$4.96\cdot10^{-7}$	$8.82\cdot10^{-9}$	$1.59\cdot10^{-6}$	$1.82\cdot10^{-8}$	$8.81\cdot10^{-9}$	$1.18\cdot10^{-6}$	$1.20\cdot10^{-6}$	$-1.29\cdot10^{-8}$	
7:40:3:V	$6.39\cdot10^{-7}$	$9.17\cdot10^{-9}$	$1.93\cdot10^{-6}$	$1.78\cdot10^{-8}$	$7.28\cdot10^{-9}$	$1.28\cdot10^{-6}$	$1.36\cdot10^{-6}$	$-7.40\cdot10^{-8}$	
7:40:3:VI	$2.06\cdot10^{-6}$	$2.33\cdot10^{-8}$	$7.71\cdot10^{-6}$	$5.62\cdot10^{-8}$	$2.58\cdot10^{-9}$	$7.20\cdot10^{-6}$	$3.51\cdot10^{-6}$	$3.69\cdot10^{-6}$	
									$6.58\cdot10^{-7}\pm 1.52\cdot10^{-6}$
7:40:4:I	$3.86\cdot10^{-7}$	$1.09\cdot10^{-8}$	$1.07\cdot10^{-6}$	$1.94\cdot10^{-8}$	$3.12\cdot10^{-8}$	$5.25\cdot10^{-7}$	$7.23\cdot10^{-7}$	$-1.98\cdot10^{-7}$	
7:40:4:II	$5.75\cdot10^{-7}$	$1.27\cdot10^{-8}$	$2.16\cdot10^{-6}$	$3.07\cdot10^{-8}$	$8.42\cdot10^{-9}$	$2.02\cdot10^{-6}$	$1.34\cdot10^{-6}$	$6.81\cdot10^{-7}$	
7:40:4:III	$6.05\cdot10^{-7}$	$1.05\cdot10^{-8}$	$3.33\cdot10^{-6}$	$3.71\cdot10^{-8}$	$4.79\cdot10^{-9}$	$4.26\cdot10^{-6}$	$1.64\cdot10^{-6}$	$2.62\cdot10^{-6}$	
7:40:4:IV	$6.96\cdot10^{-7}$	$9.31\cdot10^{-9}$	$3.73\cdot10^{-6}$	$3.21\cdot10^{-8}$	$3.18\cdot10^{-9}$	$4.69\cdot10^{-6}$	$1.56\cdot10^{-6}$	$3.13\cdot10^{-6}$	
									$1.56\cdot10^{-6}\pm 1.37\cdot10^{-6}$

The production of oxidants and hydrogen analysed in the different tests can be compared in the following graphs (Figures 5-1 to 5-3).

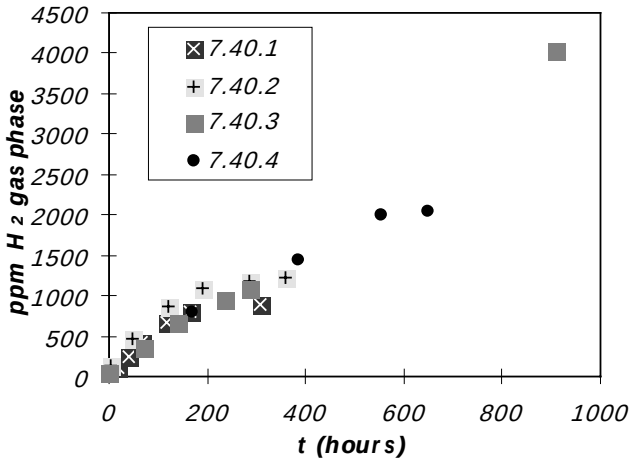

Figure 5-1. *Hydrogen concentration in the gas phase as a function of time in the four experiments.*

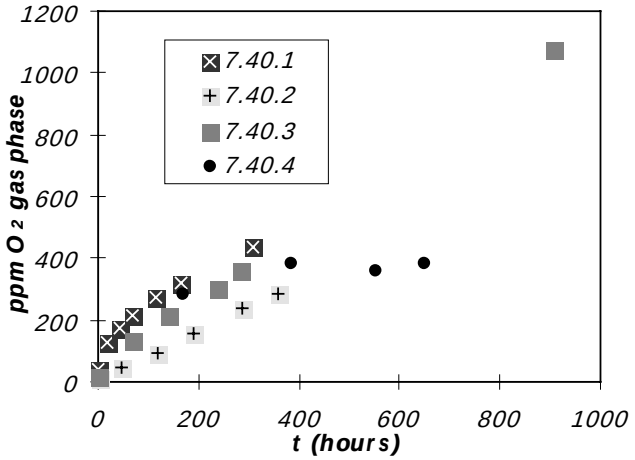

Figure 5-2. *Oxygen concentration in the gas phase as a function of time in the four experiments.*

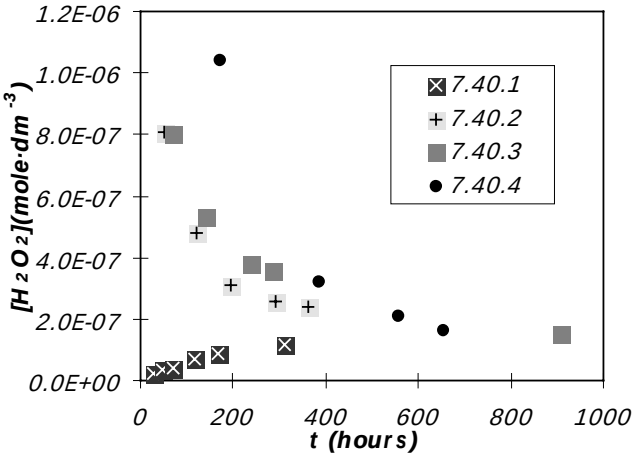

Figure 5-3. *Hydrogen peroxide concentration in solution as a function of time in the four experiments.*

In the four experiments the hydrogen concentration increases with time and shows a reproducible behaviour (Figure 5-1).

In experiments 7.40.1, 7.40.2 and 7.40.3, the oxygen concentration also shows quite a reproducible behaviour and increases continuously while in the last run (7.40.4) the concentration seems to reach a steady-state value at the end of the experimental time. This different behaviour in the last run could possibly be explained as a result of a small gas leakage. The levelling off is also observed for hydrogen in the same experiment (see Figure 5-1).

The evolution of the radiolytically generated hydrogen peroxide with time shows quite a different pattern. In the first experiment (7.40.1), the evolved hydrogen peroxide increases with time up to the 10^{-7} mole dm^{-3} level. In the subsequent runs (7.40.2 to 7.40.4), the concentrations of hydrogen peroxide decrease in a reproducible fashion, to reach a potential steady state level around 10^{-7} mole dm^{-3}, similarly to the first experiment.

The measured hydrogen peroxide concentration reflects the overall balance between: its direct production at the fuel/water interface, the reaction with the UO_2 surface plus production and recombination reactions in the bulk solution determined by β^- and γ radiolysis of water. As the contacting solution is changed, the production of hydrogen peroxide at the interface is enhanced, the generated hydrogen peroxide is scavenged by the fresh UO_2 surface and further bulk recombination reactions deplete the hydrogen peroxide concentration in solution until a steady-state concentration is obtained.

The different behaviour between the first experiment and the subsequent tests could thus be attributed to the fact that the initial fuel fragment had an oxidised UO_{2+x} less prone to generate and scavenge radiolytic hydrogen peroxide. Hence, what we observe is mainly the result of bulk recombination reactions. This oxidised surface layer is dissolved by the bicarbonate test solution and in the subsequent runs, the test solution is put in contact with a clean UO_2 fuel surface and consequently the interfacial generation and scavenging of H_2O_2 is enhanced. The comparative behaviour of hydrogen peroxide in the various tests is consistent with observations for uranium and other redox sensitive radionuclides as it will be discussed in forthcoming sections.

At this point it could be interesting to see in which way these experiments are consistent with the previous radiolytic mass balance data reported in Eriksen et al /1995/, by using deionised water as leaching solution. The following plots show a comparison of the radiolytically generated products (see Figure 5-4).

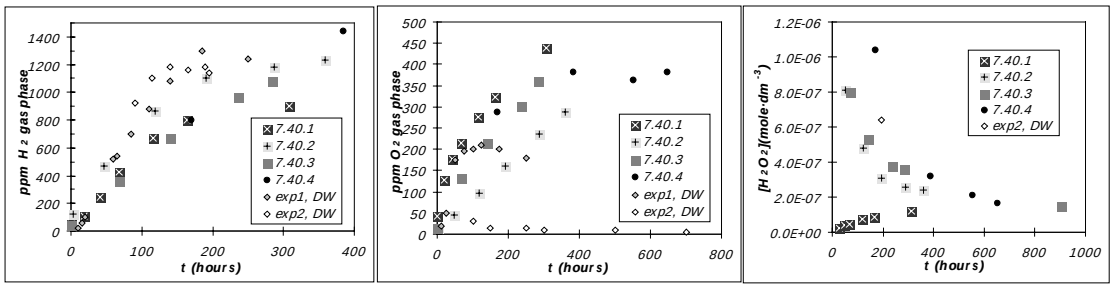

Figure 5-4. *Hydrogen (left), oxygen (middle) and hydrogen peroxide (right) concentrations as a function of time. Exp1 and exp2 data taken from Eriksen et al /1995/.*

The hydrogen concentration values appear to be somewhat higher in the experiments performed with deionised water. However, hydrogen release rates are quite consistent with the ones measured in the present work.

The comparison of oxygen behaviour deserves more attention. In the first contacting experiment with deionised water (exp1 DW) the oxygen production rates and levels are comparable to those observed in experiment 7.40.1., for the first 60-80 hours. In the subsequent contact (exp2 DW), the oxygen production is much slower and the oxygen levels are also lower. These observations strengthen the case for the critical role of the initially oxidised UO_{2+x} surface layer in determining the rates and concentrations of radiolytically generated oxidants. In this case, the spent fuel surface becomes increasingly oxidised with contact time, as no U(VI) complexing ligands are present in deionised water and no further radiolytic production of oxidants is possible as the surface becomes covered by U(VI), although this is only valid for α radiolysis. In a previous work /Eriksen et al, 1995/, we explained the different behaviour in exp2 with respect exp1 by the catalytic decomposition of radiolytically formed hydrogen peroxide on the fresh surface of exp1. This process is expected to decrease with increasing oxidation of the surface, similarly to what we observed in the 7.40.1 run of the time-resolved experiments. In the presence of carbonate in the medium the formation of an oxidised surface passivating this process is not expected. Consequently, the decrease of the oxygen concentration with time is not observed.

Finally, the hydrogen peroxide concentrations determined in the first run of the present experiments are one order of magnitude lower than the ones determined in the previous tests in deionised water. The concentrations determined in the successive runs, though, are at the same level., No further conclusions can be extracted, considering that there is only one hydrogen peroxide determination reported from the previous experiments carried out in deionised water.

5.1.2 Radionuclide concentrations in solution

As a first approximation, we have calculated the ratios between the minor radionuclides and uranium determined in solution. These are compared to the nominal inventory ratios in order to establish their potential co-dissolution with the uranium(IV) dioxide matrix The experimental ratios for each test with the corresponding standard deviation, together with the ratios calculated based on the inventory of the fuel sample are given in Figure 5-5.

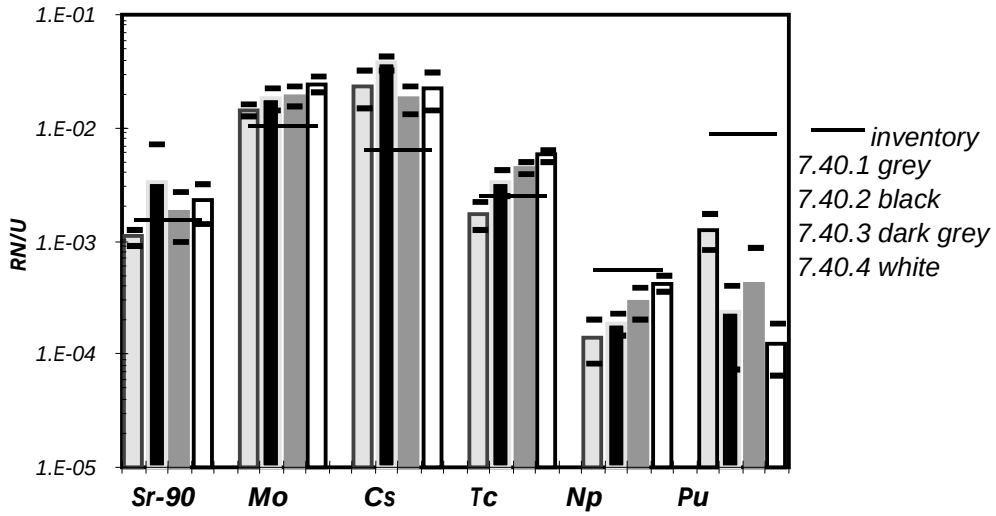

Figure 5-5. *Calculated ratios in solution with respect the U in each experimental test and calculated ratio based on the inventory of the fuel sample. The brackets indicate the standard deviation in the solution ratios as a result of the analytical determinations.*

As we can see from Figure 5-5, the calculated ratio from the dissolution data is similar to the one based on the inventory of the fuel sample for Sr-90, while Tc and Mo, seem to be close within the experimental error. This agreement could indicate that the dissolution of these elements is controlled by matrix dissolution. This has been previously observed when studying the evolution of these radionuclides as a function of time. This behaviour expected for Sr, it is somewhat surprising for Mo and Tc since these elements are usually found as separated metallic inclusions in the fuel.

In the case of Cs, the larger Cs/U ratio measured in solution with respect to the inventory is also expected based on its preferential location at grain boundaries /Forsyth and Werme, 1991; Forsyth, 1995/.

Np gives in the initial runs, lower than inventory Np/U ratios. However, as the subsequent runs proceed, the Np/U ratios approach the inventory level.

Finally, Pu consistently gives lower than expected ratios in solution. This would indicate that additional solubility controlling mechanisms operate for this radionuclide, i.e. secondary phase precipitation following the initial congruent release. This has already been proposed in our former analysis of the early contact times of the very long time leaching experiments /Bruno et al, 1998/.

Y and Nd have not been included in this analysis as they do not shown any clear relationship with the inventory ratios.

5.1.3 Estimation of the redox condition of the experiments

The second step in the modelling of the experimental data consisted on the analysis of the various redox pairs present in solution and the calculation of a nominal pe in the aqueous phase. The calculations have been performed by means of the radiolytic data based on the electron balance in the aqueous phase as well as by considering several

redox couples based on solution data. We define below the different redox systems taken into account in calculating the nominal pe in the aqueous phase.

- **pe calculation based on the electron balance in the aqueous phase**

  The oxidising capacity of the solution (OXC) has been defined as:

$$OXC = 4 \times [O_2]aq + 2 \times [H_2O_2]aq + 2 \times [U(VI)]aq - 2 \times [H_2]aq \qquad (5\text{-}3)$$

  where U (VI) denotes the uranium released to the solution due to the oxidation of UO_2. In the previous equation only uranium has been considered as redox sensitive element to calculate the electron balance based on the fact that this radionuclide is the major component of the fuel matrix.

  Reordering the previous equation and taking into account the corresponding equilibria reactions, we obtain the following expression as a function pH and pe and of the bicarbonate concentration of the system.

$$\begin{aligned} OXC = {} & 4 \times \frac{K_H(O_2)}{k_{O_2} \times [H^+]^4 \times [e^-]^4} + 2 \times \frac{1}{k_{H_2O_2} \times [H^+]^2 \times [e^-]^2} + \\ & + 2 \times \frac{keq \times [HCO_3^-]^3}{[H^+]^3 \times [e^-]^2} - 2 \times K_H(H_2) \times [H^+]^2 \times [e^-]^2 \end{aligned} \qquad (5\text{-}4)$$

  where $K_H(O_2)$ and $K_H(H_2)$ denote the Henry constant of oxygen and hydrogen respectively; k_{O2} and k_{H2O2} denote the equilibrium constant of oxygen and hydrogen peroxide to water respectively and keq denotes the equilibrium constant of the following reaction:

$$UO_2(s) + 3HCO_3^- \Leftrightarrow UO_2(CO_3)_3^{4-} + 3H^+ + 2e^- \qquad (5\text{-}5)$$

  where the uranyl tri-carbonate aqueous complex is the predominant uranium species in the aqueous phase under these experimental conditions.

- **pe calculation based on uranium equilibrium according to equation 5-5**

  in such case, the pe of the system can be expressed as:

$$pe = (\log[UO_2(CO_3)_3^{4-}] - 3 \times pH - 3 \times \log[HCO_3^-] - \log keq) / 2 \qquad (5\text{-}6)$$

- **pe calculation based on technetium equilibria according to the following reactions:**

$$Tc(m) + 4H_2O \Leftrightarrow TcO_4^- + 8H^+ + 7e^- \qquad (5\text{-}7)$$

where the pe can be expressed as:

$$pe = (\log[TcO_4^-] - 8 \times pH - \log keq) / 7 \quad (5\text{-}8)$$

and

$$TcO_2 \cdot 1.63H_2O(s) + 0.37H_2O \Leftrightarrow TcO_4^- + 4H^+ + 3e^- \quad (5\text{-}9)$$

where the pe in such case can be expressed as:

$$pe = (\log[TcO_4^-] - 4 \times pH - \log keq) / 3 \quad (5\text{-}10)$$

where keq in all cases denotes the equilibrium constants of the respective reactions described above.

The results of these calculations are given in the next plots (Figure 5-6).

The pe values calculated using uranium and technetium equilibria are quite close in all the runs but slightly lower than the pe values calculated from the radiolytic products electron balance. On the other hand, the pe calculated by assuming TcO_2/TcO_4^- result in higher redox potentials than the ones calculated by using the radiolytic products and the uranium (VI)/(IV) redox pair.

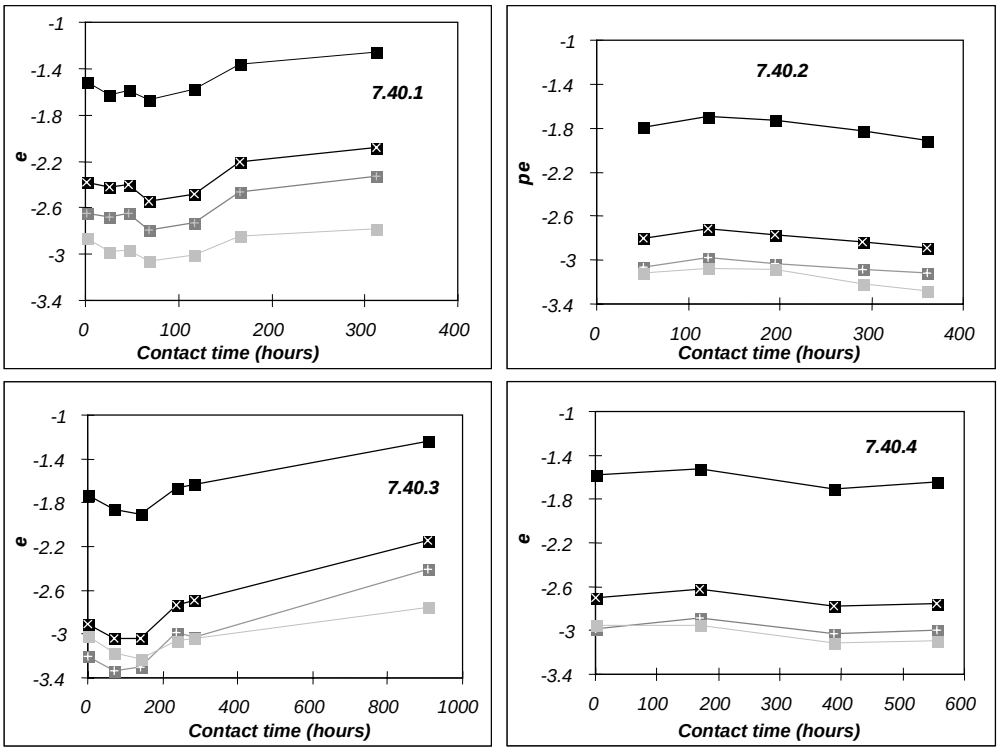

Figure 5-6. *Calculated pe in experiments 7.40.1 (left upper), 7.40.2 (right-upper), 7.40.3 (left lower) and 7.40.4 (right lower). Black squares with white crosses stand for electron balance values; dark grey squares with white crosses stand for uranium equilibrium values; black squares correspond to TcO_2 equilibrium values and light grey squares correspond to Tc(m) equilibrium values.*

The agreement between calculated pe when considering the UO_2(s)/U(VI) and Tc(m)/ TcO_4^- indicate that redox equilibrium is attained in the aqueous phase. The difference (25 mV approximately) with the calculated pe based on the electron balance of the radiolytic products can be considered to be within the experimental error. This would indicate that an overall redox state can be estimated for the experimental system.

The larger discrepancy within calculated pe values are observed in the first experiment (7.40.1). This difference is attributed to the existence of a initially oxidised surface layer in the fuel specimens prior to the first dissolution experiment. The larger release of uranium(VI) in the first run leads to a higher calculated redox potential with respect the subsequent three runs. This will have further implications when discussing the behaviour of minor radionuclides,

5.1.4 Calculation of the saturation state of the various radionuclides with respect to solubility limiting phases

An equilibrium modelling approximation has been used in order to determine to what extent the released radionuclides are solubility limited with respect to the primary source, the UO_2 spent fuel matrix, or some secondary phase formation. In order to do so, the saturation indexes of the most favoured pure solid phases have been calculated by using the analytical data from the various experiments.

The saturation index of a solution with respect a solid phase is defined according to the following equation:

$$S.I. = \log (Q/Ks) \qquad (5\text{-}11)$$

where Q denotes the ionic product of solid forming components in solution and Ks denotes the solubility constant for the reaction. As an example, if the general reaction for the formation of the solid phase is:

$$A + B \Leftrightarrow AB(s)$$

Then Ks = [A][B] in equilibrium and the analytical concentration product is defined as $Q = [A]_{an}[B]_{an}$.

If Q>Ks, then S.I.>0 and the system is oversaturated with respect the solid considered. If Q=Ks, then S.I.=0 and the system is in thermodynamic equilibrium. Finally, if Q<Ks, then S.I.<0 and the system is undersaturated with respect the solid phase under consideration.

Some of the elements involved undergo redox transitions and consequently the redox state of the solution has to be established in the calculations. For this purpose, the average values of the calculated pe according to the UO_2/U(VI) and Tc(m)/TcO_4^- equilibria were considered for each experiment. The results are discussed element by element in the following sections.

Uranium

As we have already pointed out, the concentration of uranium in solution under the experimental conditions and is limited by the degree of oxidative dissolution of the spent fuel matrix. This is illustrated in Figure 5-7 where all solutions appear to be close to equilibrium with UO_2. Only, in the first run the determined uranium concentrations are slightly oversaturated. This is a further indication of the existence of an oxidised UO_{2+x} layer.

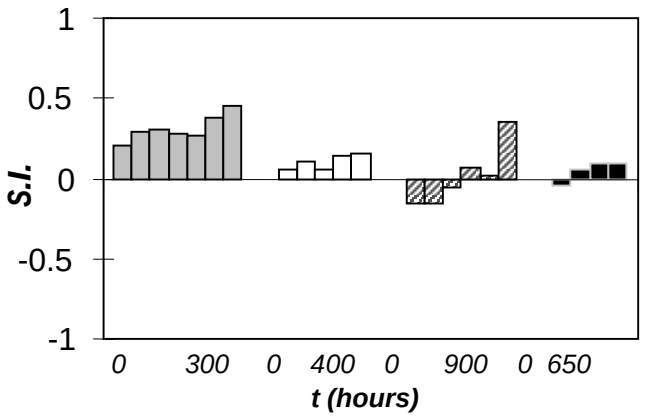

Figure 5-7. *Saturation indexes of $UO_2(s)$ in the four runs. Grey bars:7.40.1; White bars:7.40.2; Dashed bars:7.40.3 and Black bars:7.40.4.*

Strontium

Strontianite is thermodynamically the most favourable solid phase for Sr in the experimental conditions. However, as shown in Figure 5-8, all solutions are clearly undersaturated with respect to this phase. Hence, the release of this element in solution is not merely controlled by its individual solubility.

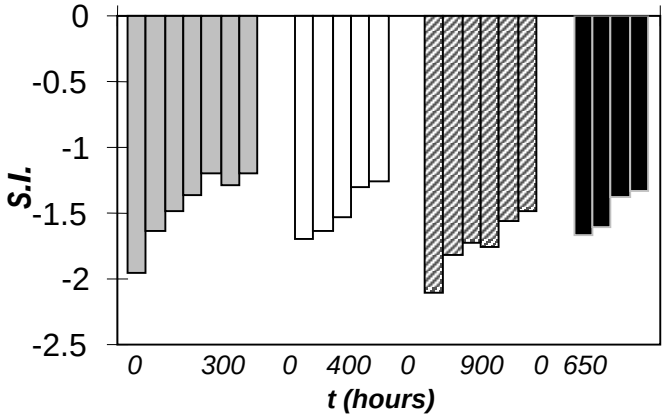

Figure 5-8. *Saturation indexes of strontianite ($SrCO_3(s)$) in the four runs. Grey bars:7.40.1; White bars:7.40.2; Dashed bars:7.40.3 and Black bars:7.40.4.*

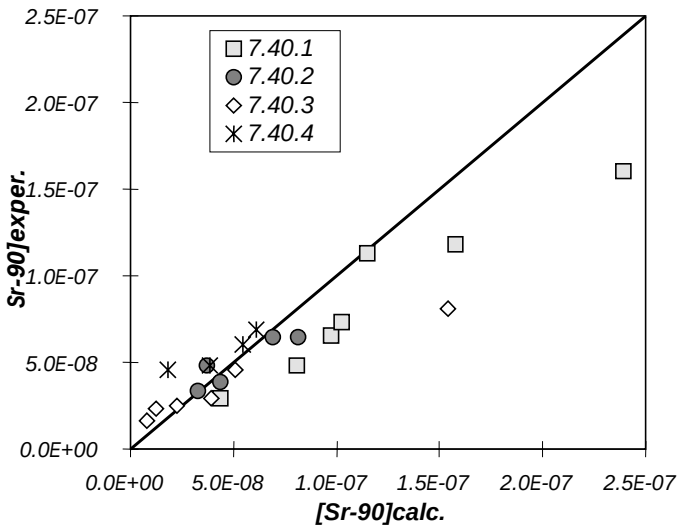

***Figure 5-9**. Strontium concentrations determined in the leaching solution versus strontium concentrations calculated assuming a congruent co-dissolution process.*

We attempted to ascertain if the release of Sr is controlled by its congruent dissolution with the fuel matrix. As we can see in Figure 5-9, the Sr/U relation between the measured and calculated ratio, according to inventory, are close to one (solid line). These observations constitute an additional support to the congruent behaviour of Sr with U, and the possibility of using this element as an indicator of matrix dissolution.

Only in the first run a clear deviation from the expected behaviour is observed with a lower than expected release of Sr. This result is contrary to the one expected if Sr-90 would be enriched at grain boundaries by migration of its short-lived Kr and Rb precursors /Forsyth, 1997/, and more accessible to dissolution in the fresh samples.

The Sr behaviour could be explained by assuming that this radionuclide is not present at the inventory ratio in the UO_{2+x} oxidised surface layer of the unreacted fuel sample. Once this layer is depleted, Sr dissolves congruently with uranium.

Caesium

Caesium, as expected, is not solubility limited under the experimental conditions. The concentration of caesium in the contacting solutions follow similar trends as Sr and U (see Figures 4-5 and 4-7).

The calculated ratio between this radionuclide and U in the aqueous phase is approximately one order of magnitude larger than the one given by the inventory of the solid sample (Figure 5-5). The non-congruent co-dissolution of caesium with respect to uranium is a result of the location of this radionuclide in the phase boundaries, due to its migration to the fuel/clad gaps during irradiation in the reactor /Forsyth and Werme, 1991/. According to Forsyth /1995/, both Cs and I show a release behaviour similar to the inert gases, Kr and Xe. Hence, fission gas release models can be applied to estimate the magnitude of the effect. Forsyth and Werme /1991/ determined also a rapid release during the first few weeks of long term spent fuel dissolution experiments. After this instant release, they observed a decrease in the release rate of this radionuclide until they got to a steady level. This is all consistent with our present observations.

Plutonium

The observed plutonium concentrations in solution suggest that additional processes to matrix dissolution govern its overall behaviour. In the first experiment 7.40.1, uranium and plutonium seem to have a similar dissolution behaviour (Figures 4-5 and 4-6 (right) for comparison). However, the Pu to U ratio calculated in the first run from the experimental concentrations is lower than the inventory one (Figure 5-5). Furthermore, once the oxidised surface layer of the fresh sample is depleted, the dissolved Pu concentrations decrease with time, as it is observed in the runs 7.40.2 to 7.40.3.(Figure 5-5).

This is a clear indication of the precipitation of a secondary phase controlling the Pu concentrations in solution. In order to find out which are the most probable solid phases we have calculated the saturation state of the different experimental solutions with respect to the most probable secondary phases.

Under the experimental conditions Pu is present mainly as Pu(IV), hence solid phases of this oxidation state have been considered. According to previous work /Bruno et al, 1998/ the short term behaviour of Pu from spent fuel leaching appears to be initially controlled by the formation of a $Pu(OH)_4$ poorly ordered phase (denoted as $Pu(OH)_4$(coll)), followed by the ageing of this phase to a more stable amorphous $Pu(OH)_4$(am) phase. Consequently, the relative stability of these phases in the present experimental conditions have been explored by calculating their saturation indexes under these experimental conditions as presented in Figure 5-10.

The calculations indicate that Pu is in equilibrium with respect a colloidal plutonium hydroxide only in the first experiment (Figure 5-10, left). In the subsequent runs, the observed Pu concentrations are slightly over-saturated with respect to $Pu(OH)_4$(am) which is an indication that the ageing process could be taking place.

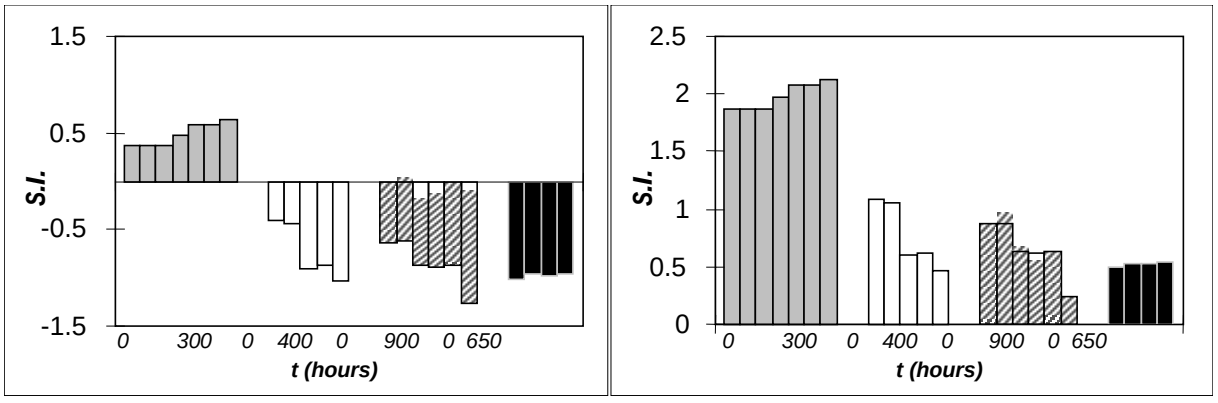

Figure 5-10. *Saturation indexes of $Pu(OH)_4$(col) (left) and $Pu(OH)_4$(am) (right) in the four runs, solubility constants taken from Bruno et al /1998/. Grey bars:7.40.1; White bars:7.40.2; Dashed bars:7.40.3 and Black bars:7.40.4.*

Neptunium

The analysis of the primary data indicate that neptunium follows the behaviour of uranium in the four tests. This is, they are congruently released. However, the calculated ratios from solution data are somewhat lower than the inventory ratio (Figure 5-5). This could initially be the effect of the relative enrichment of U with respect to Np on the initially oxidised surface layer. As this layer is dissolved, the Np/U ratio in solution approach the inventory ratio.

Based on the equilibrium calculations, the neptunium concentrations in solution are undersaturated with respect to $Np(OH)_4(s)$ for the four tests but they approach equilibrium as the dissolution reaction proceeds. (Figure 5-11).

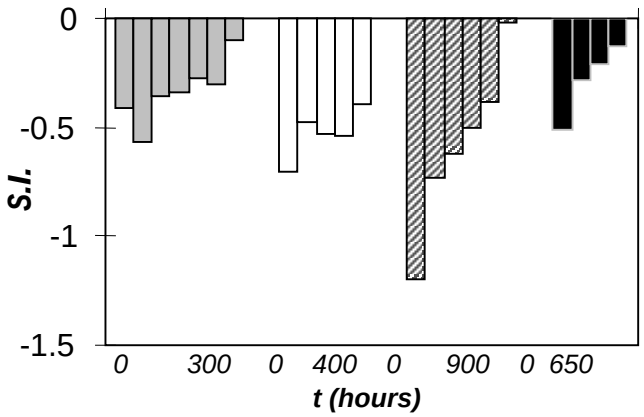

Figure 5-11. *Saturation indexes of $Np(OH)_4(s)$ in the four runs. Grey bars:7.40.1; White bars:7.40.2; Dashed bars:7.40.3 and Black bars:7.40.4.*

These results could indicate an initial congruent dissolution of Np with U, followed by the precipitation of $Np(OH)_4(s)$ as the reaction proceeds. This solubility control has been also proposed in previous experimental studies /Forsyth and Werme, 1992; Forsyth, 1997/.

Molybdenum and technetium

As expected, Mo is not solubility limited under the experimental conditions of the present experiments. This is mainly due to the formation of MoO_4^- in the aqueous phase as a result of the presence of oxidants at the spent fuel/water interface.

Based on the redox modelling previously performed, the concentration of Tc in the aqueous phase is governed by the oxidative dissolution of metallic particles located in the fuel matrix. The saturation indexes calculated when considering equilibrium with Tc(m) is shown in Figure 5-12.

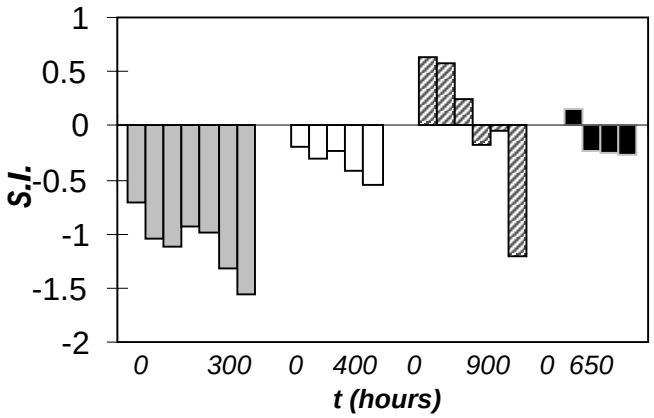

Figure 5-12. *Saturation indexes of Tc(m) in the four runs. Grey bars:7.40.1; White bars:7.40.2; Dashed bars:7.40.3 and Black bars:7.40.4.*

The release of both elements from the fuel matrix follows the same trend as uranium as we can observe when comparing Figures 4-5 and 4-8. The agreement between the observed ratios in solution and the inventory (Figure 5-5) indicate that they dissolve congruently with the oxidative dissolution of the matrix.

This is illustrated in Figures 5-13 and 5-14, where the solution concentrations have been compared to the expected concentrations assuming congruent release with uranium according to the inventory.

The data concerning molybdenum (Figure 5-13) shows an increased deviation from the theoretical line at larger Mo concentrations. This behaviour could indicate a differentiated mechanism for Mo dissolution as the reaction proceeds.

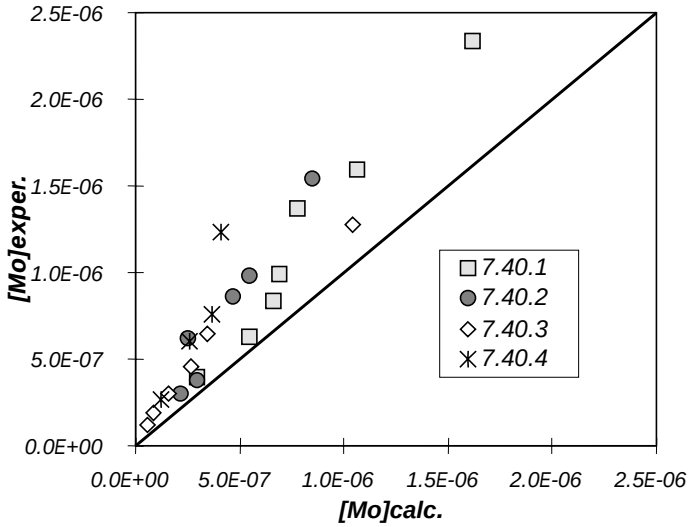

Figure 5-13*. Molybdenum concentrations determined in the leaching solution versus concentrations calculated assuming a congruent co-dissolution process.*

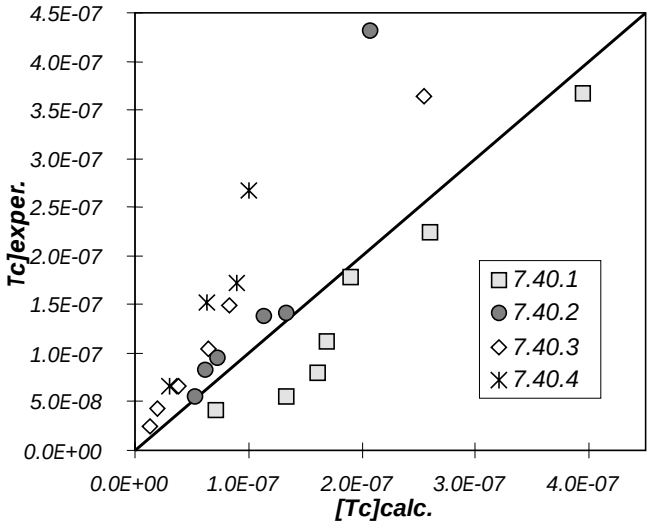

Figure 5-14. *Technetium concentrations determined in solution versus concentrations calculated assuming a congruent co-dissolution process according to the inventory.*

The comparison of calculated and measured data indicates that Tc dissolves congruently according to the inventory ratio, within the experimental uncertainty. (Figure 5-14).

Mo can be found in the spent fuel forming metallic particles and also forming oxide precipitates /Kleykamp, 1988; Forsyth, 1995; Hanson, 1998/. Tc is usually located in metallic inclusions. These radionuclides have been also identified as micron size particles at or between the fuel grain boundaries and at fission gas bubbles /Forsyth, 1997/. Therefore, their release could expected to be controlled by several different processes to the matrix dissolution.

Gray /1998/ performed various flow-through tests using fuel samples with different degrees of oxidation. Tc results from these experiments were quite surprising. In some tests he observed that Tc dissolved slower than the matrix, while in other tests he obtained that Tc dissolved nearly congruently with the matrix dissolution from both oxidised and non-oxidised fuel samples. The author relates this behaviour to the location of this fission product as metallic inclusions. However, the distribution of these inclusions in the fuel seem to depend on temperature and burnup /Kleykamp, 1988/. Consequently, the variation in the Tc distribution may contribute to the variation in the Tc dissolution mechanisms.

Forsyth and Werme /1992/ and Forsyth /1997/ stated that under oxidising conditions, the release of technetium and molybdenum is probably controlled only by oxidation of these inclusions. This statement is in agreement with the findings of the present work.

In order to study to which extent the behaviour of these two redox sensitive elements is related, we have studied the potential correlation in the dissolution behaviour of both radionuclides. For this purpose, we have calculated the expected technetium concentrations according to a congruent co-dissolution process with molybdenum. The results are given in Figure 5-15.

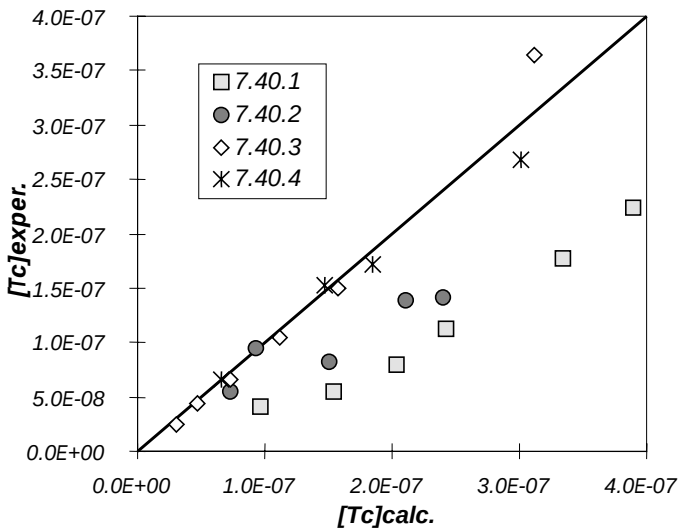

***Figure 5-15**. Technetium concentrations determined in the leaching solution versus concentrations calculated assuming a congruent co-dissolution process with molybdenum.*

The data in Figure 5-15 indicates a lower than expected release of Tc assuming a congruent dissolution process with Mo in the first two runs, while ideal co-dissolution behaviour is approached in the subsequent runs. Molybdenum has the highest affinity for oxygen, and consequently it oxidises first in the metallic inclusions /Kleykamp, 1988/. The oxidation of the fuel and of the exposed metallic particles during air storage before the start of the corrosion tests could explain the major oxidation of molybdenum with respect technetium and consequently its major release in the first and second. This is agreement with previous observations by Forsyth /1997/, who also attributes the initial major release rate obtained in his experiments to this previous oxidation due to air storage of the fuel specimens.

In the third and four runs, molybdenum and technetium dissolve at the same rate. This behaviour could be consistent with a process of gradual infiltration of the microcracks and grain boundaries, oxidation of the particles and slow return to and mixing with the main solution. Forsyth /1997/ used the same reasoning to explain the decrease on the fractional release rates with time after the initial Mo pulse.

Hence, according to the previous discussions the present experimental observations indicate that Mo and Tc will co-dissolve congruently as the metallic particles become oxidised.

Yttrium and neodymium

The primary analysis of the data shows that the mechanisms controlling the release of these lanthanides are not solely related to matrix dissolution. These results are somewhat unexpected as it is assumed that the lanthanide elements are homogeneously dispersed in the fuel matrix /Forsyth, 1997/. As consequence, a congruent dissolution with the matrix could be expected.

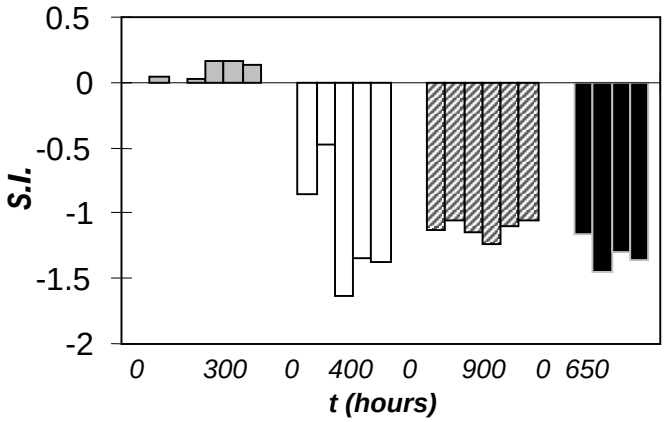

Figure 5-16. *Saturation indexes of $NdOHCO_3(s)$ in the four runs. Grey bars:7.40.1; White bars:7.40.2; Dashed bars:7.40.3 and Black bars:7.40.4.*

Yttrium and neodymium are in general under saturated with respect any pure solid phase in the present experiments. However, neodymium is close to equilibrium with $NdOHCO_3(s)$ in the first run but clearly undersaturated in the subsequent runs, as we can see in Figure 5-16.

Similarly, no conclusion can be drawn about the processes controlling the release of yttrium from the fuel matrix since it is undersaturated with respect any pure solid phase. However, due to the chemical similarity between both radionuclides, a co-precipitation process of Y onto the neodymium mixed carbonate solid phase has been considered in this modelling work. The analysis of the data indicated that this process is not likely to control the Y concentrations in solution.

Forsyth /1997/ suggests that the lanthanide and actinide elements could be co-precipitated with or scavenged by uranium deposited, in such case, these radionuclides would be enriched in the deposit with respect the uranium. An attempt to confirm this enrichment effect was performed by Forsyth et al /1990/ by analysing small traces of dehydrated schoepite scraped from a fuel specimen corroded in deionised water, however, no convincing evidence of actinide enrichment was observed.

As it has been previously shown, the release of uranium in these experiments is only controlled by the oxidative dissolution of the matrix and no secondary uranium phase is formed in these experiments. Hence, such a co-precipitation process is clearly not working under the present circumstances.

Otherwise, sufficient dissolution data concerning other rare earth elements are not available in the present experiments in order to consider other mechanisms controlling the solubility of these radionuclides.

5.2 Long time experiments

In order to analyse the data from these experiments, in the context of the previous observations, we will have to keep on mind that these long-time data are the natural temporal continuation of the data collected in the short term time-resolved tests. This is illustrated in Figure 5-17 where the hydrogen measurements of experiments 7/7 and 3/3,

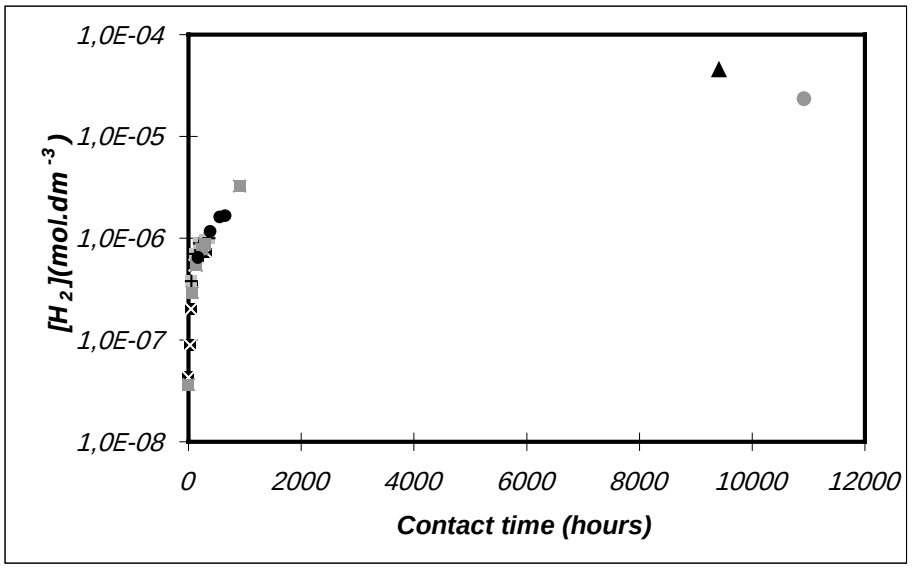

Figure 5-17. *Measured hydrogen concentrations in the time resolved experiments (7.40.1–7.40.4) and experiments 3/3 (black triangles) and 7/7 (grey dots).*

performed in 10 mM bicarbonate solution are overimposed to the results from the time-resolved runs.

Because, of the much longer contact times involved in these test which were basically run in similar chemical conditions than the time-resolved, we expect to observe the final result of some of the processes already pointed out in the previous discussion. Unfortunately, the longer experimental time increase also the possibility of perturbation of the test solutions by gas leakage and other unwanted effects.

5.2.1 Radiolysis products

The first step in this modelling work has been to find correlations between the different species involved in the system. For this purpose, we have analysed the major components of the system. This includes the radiolysis products, hydrogen, oxygen and hydrogen peroxide as well as the carbonate content of each experiment. In this sense, some interesting results have been obtained.

Concentrations of oxygen and hydrogen in the aqueous phase have been calculated based on the measurements performed in the gas phase taking into account the Henry constant for both gases respectively, similarly to the previous experiments (eq. 4-1).

Figure 5-18 is a plot of the hydrogen concentrations in front of the oxygen concentrations for all the experimental tests. As we can observe, the concentration of oxygen increases when increasing the hydrogen concentration. However, the O/H correlation is lower than 1:1. The measured oxygen concentration in the experiment performed in bicarbonate solution (denoted 3/3), was significantly lower than the hydrogen concentration measured in the same experiment. This experiment is not included in this Figure.

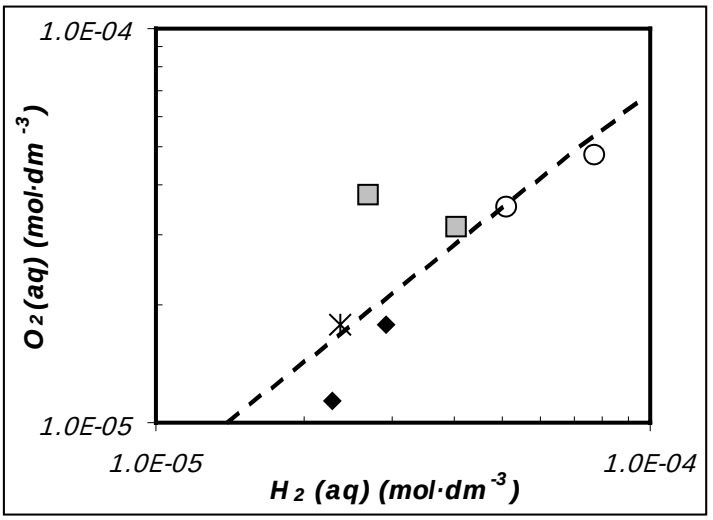

Figure 5-18. *Correlation between O_2(aq) and H_2(aq) concentration in the leaching solution (white rounds: DW, grey squares: Allard GW, black diamonds: bicarbonate ($2 \cdot 10^{-3}$ M) solution and crosses: bicarbonate ($1 \cdot 10^{-2}$ M) solution).*

The oxygen and hydrogen peroxide concentrations measured in the experiments are plotted in Figures 5-19 and 5-20 respectively as a function of the total carbonate concentration of the system.

The data plotted in both figures indicate that the oxygen and the hydrogen peroxide concentrations decrease when increasing the carbonate content of the system. This behaviour can be explained by a higher recombination of different radicals with the consequent decrease of oxidants generation when carbonate is present in the system. This fact remains to be confirmed by additional experiments, as the results for the duplicate exp. 7/7, at 10 mM bicarbonate give oxygen concentrations roughly in the same level as the ones performed in deionised water and 2 mM bicarbonate.

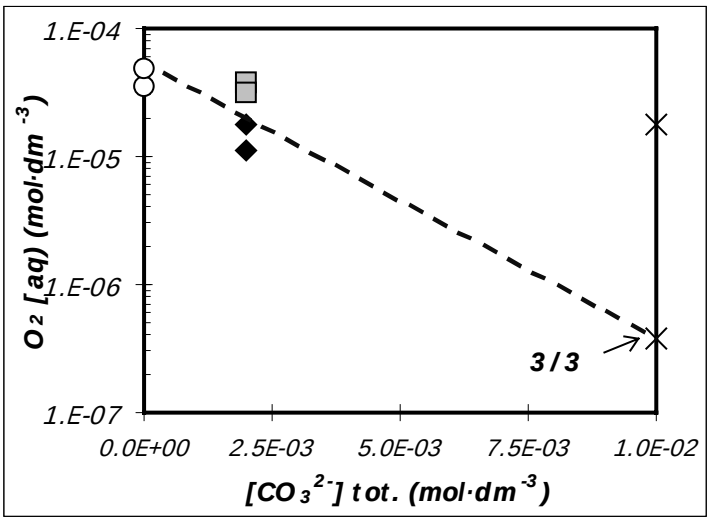

Figure 5-19. *Correlation between O_2(aq) and CO_3^{-2} total concentration in the leaching solution (white rounds: DW, grey squares: Allard GW, black diamonds: bicarbonate ($2 \cdot 10^{-3}$ M) solution and crosses: bicarbonate ($1 \cdot 10^{-2}$ M) solution).*

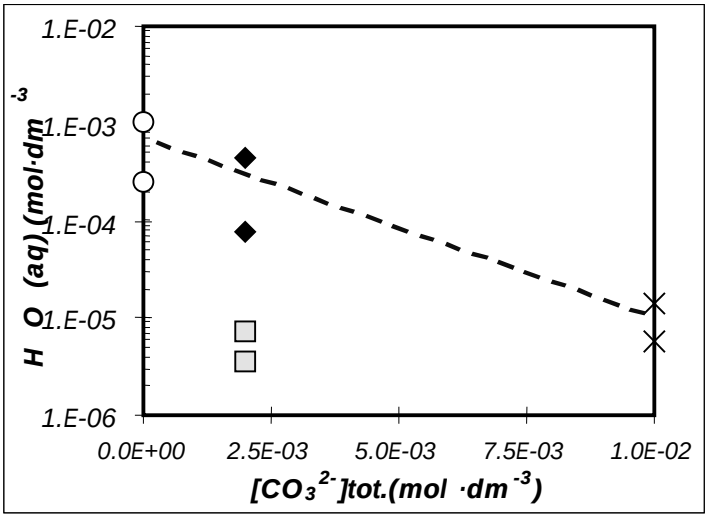

Figure 5-20. *Correlation between H_2O_2(aq) concentration and CO_3^{-2} total concentration in the leaching solution (white rounds: DW, grey squares: Allard GW, black diamonds: bicarbonate ($2 \cdot 10^{-3}$ M) solution and crosses: bicarbonate ($1 \cdot 10^{-2}$ M) solution).*

A more striking observations is made in Figure 5-20, where the hydrogen peroxide concentration proves to be consistently lower in the experiments performed with Allard groundwater. The different behaviour with respect the other tests indicates that the presence of other anions in the system, mainly chloride, could have an effect on the generation of hydrogen peroxide by the radiolysis of water.

The net production of oxidants and reductants in each experiment is reflected in the next graph (Figure 5-21). The electron balance has been calculated as in the previous data treatment (Section 5.1.1), by considering the hydrogen, oxygen and hydrogen peroxide concentrations measured in the gas and aqueous phases according to equation 5-1. As it is shown in Figure 5-21, white bars, the balance is clearly oxidant in all the experiments, with one exception, experiment 3/3 performed with a bicarbonate solution,

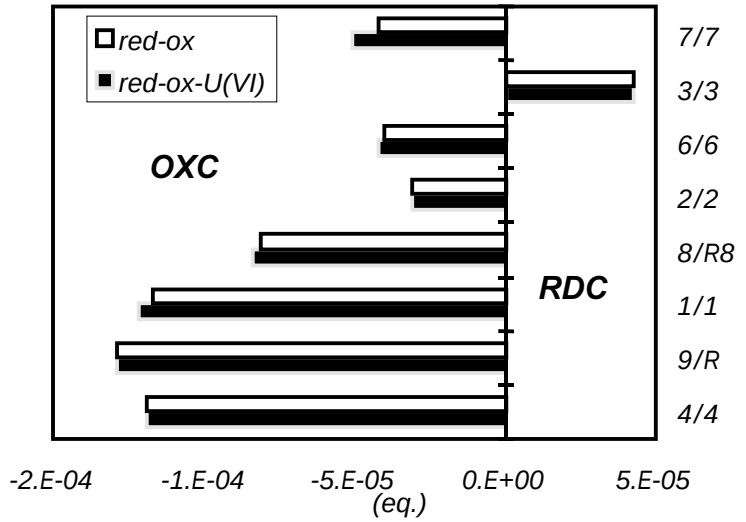

Figure 5-21. *Electron balance calculated by using the experimental data OXC stands for excess of oxidants in the system and RDC stands for excess of reductants in the system.*

where a lower oxygen concentration was measured at the end of the experiment with respect the other three. The overall balance is not changed by considering the contribution of the dissolved U(VI) (black bars in the same graph).

The unbalance calculated in all these systems could be explained by the radicals generated by recombination reactions to give a net electron balance of these systems. The complexity of the system does not allow any further analysis.

5.2.2 Radionuclide concentrations in solution

As in the previous section, the primary analysis of the data included finding the possible correlations between the different elements measured in solution.

The correlation between the different elements measured in solution, mainly in front of uranium, are given in Figures 5-22 to 5-27. In Figure 5-22 we can observe, similarly to the findings from the previous section, a satisfactory correlation between Sr and U. This could give additional support to the hypothesis of Sr co-dissolution with uranium.

The lack of correlation obtained in three of the experiments could indicate that other processes are responsible for the release of both elements in solution.

In deionised water, the release of uranium is controlled by the secondary precipitation of schoepite and consequently, Sr is expected to be at higher concentrations than the ones given by the Sr/U inventory ratio. In bicarbonate solutions, and particularly at lower concentrations, some of the Sr in solution could be the result of impurities in the stock solutions, rather than the result of Sr-90 release from the fuel. This effect is minimised in the higher carbonate concentrations where the increased release of Sr from the fuel masks the contribution from the stock solutions.

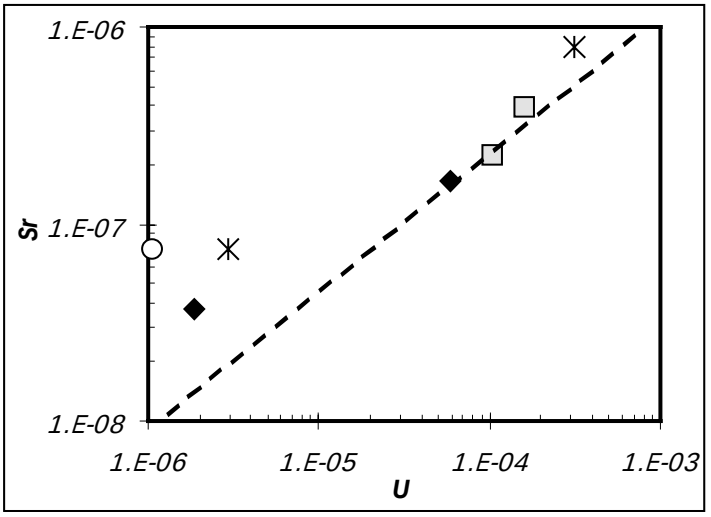

Figure 5-22. *Correlation between Sr and Uranium concentrations in the leaching solution (white rounds: DW, grey squares: Allard GW, black diamonds: bicarbonate ($2 \cdot 10^{-3}$ M) solution and crosses: bicarbonate ($1 \cdot 10^{-2}$ M) solution).*

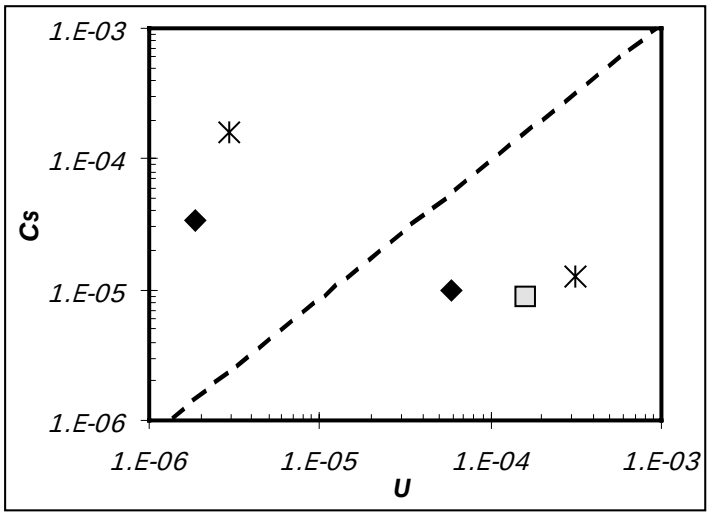

Figure 5-23. *Correlation between Cs and U concentrations in the leaching solution (white rounds: DW, grey squares: Allard GW, black diamonds: bicarbonate ($2 \cdot 10^{-3}$ M) solution and crosses: bicarbonate ($1 \cdot 10^{-2}$ M) solution).*

As expected, caesium is released from the matrix by differentiated mechanisms to uranium, as shown by the lack of correlation between Cs and U, as presented in Figure 5-23. As we have previously discussed, caesium is located in the grain boundaries and it is more accessible to dissolution than the matrix itself. No solubility limit is expected for this element under the present conditions.

A comparison of the Pu and Np concentrations in solution with respect to uranium is given in Figures 5-24 and 5-25, respectively. As we can observe in Figure 5-24, there is a poor correlation between Pu and U in all the experimental tests.

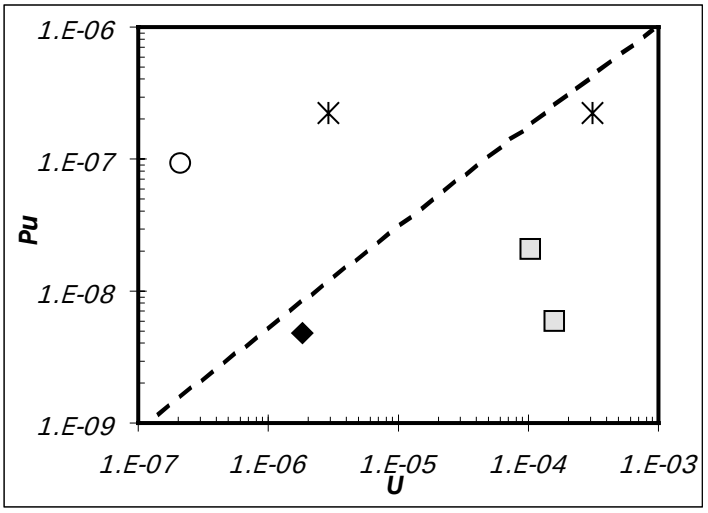

Figure 5-24. *Correlation between Pu and U concentrations in the leaching solution (white rounds: DW, grey squares: Allard GW, black diamonds: bicarbonate ($2 \cdot 10^{-3}$ M) solution and crosses: bicarbonate ($1 \cdot 10^{-2}$ M) solution).*

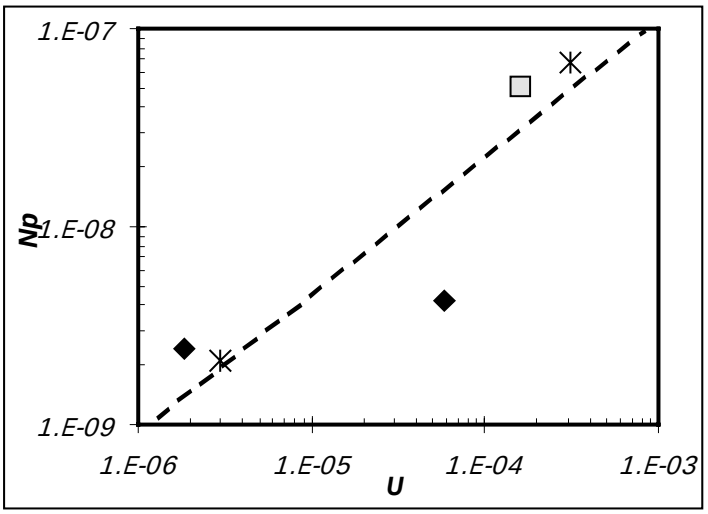

Figure 5-25. *Correlation between Np and U concentrations in the leaching solution (white rounds: DW, grey squares: Allard GW, black diamonds: bicarbonate ($2 \cdot 10^{-3}$ M) solution and crosses: bicarbonate ($1 \cdot 10^{-2}$ M) solution).*

We obtain quite a good correlation between Np and U in solution as shown in Figure 5-25. The correlation obtained between Np and U could indicate a congruent dissolution of this actinide with the major component of the fuel matrix. In agreement with the findings from the previous section.

Finally, technetium and molybdenum behave in a different way with respect to uranium according to the correlations showed in Figures 5-26 and 5-27 respectively. Mo does not dissolve congruently with the matrix (Figure 5-27), while Tc appears to co-dissolve with the spent fuel matrix in most of the cases (Figure 5-26).

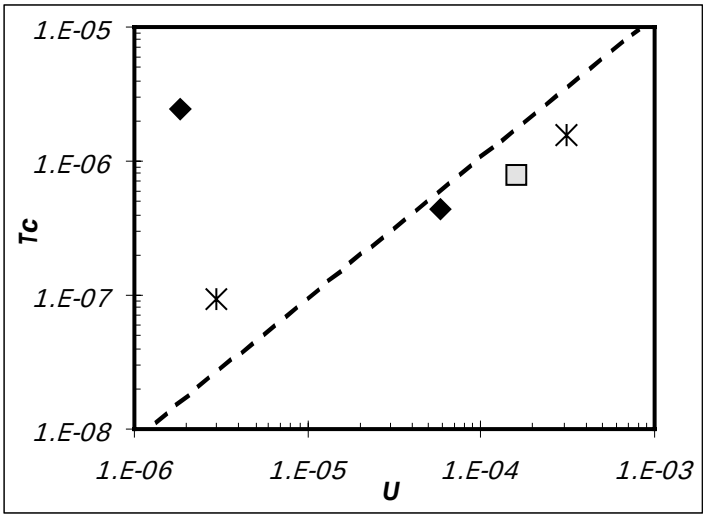

Figure 5-26. *Correlation between Tc and U concentrations in the leaching solution (white rounds: DW, grey squares: Allard GW, black diamonds: bicarbonate ($2 \cdot 10^{-3}$ M) solution and crosses: bicarbonate ($1 \cdot 10^{-2}$ M) solution).*

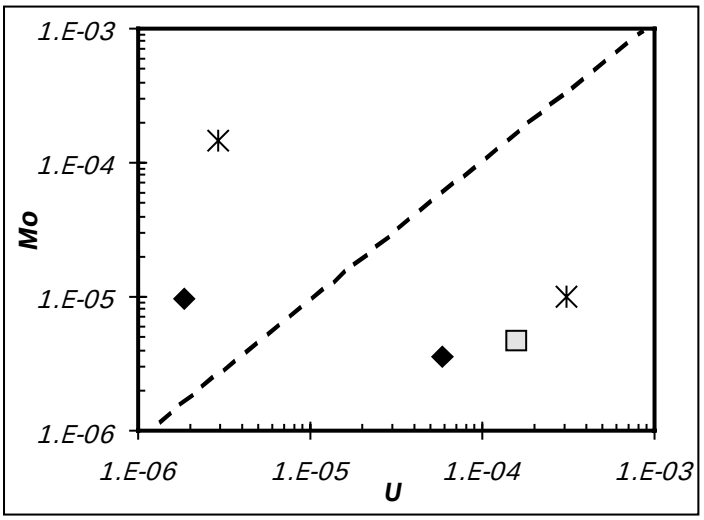

Figure 5-27. *Correlation between Mo and U concentrations in the leaching solution (white rounds: DW, grey squares: Allard GW, black diamonds: bicarbonate ($2 \cdot 10^{-3}$ M) solution and crosses: bicarbonate ($1 \cdot 10^{-2}$ M) solution).*

The ratios of the different elements measured in solution with respect to uranium have been calculated in each experiment. This has been done following the same methodology applied for the time-resolved experiments, The results are given in Figure 5-28, together with their theoretical ratios based on their inventory.

In most of the experiments the observed Pu/U concentration ratios are within 1 to 3 orders of magnitude below the inventory ratio. This indicates that, in agreement with the findings from the time-resolved experiments, the secondary precipitation of $Pu(OH)_4(s)$ controls the release of this element. Only, in one of the test with the largest bicarbonate concentration (7/7, $[HCO_3^-]$ = 0.01 M), the measured Pu concentration is over the inventory ratio. This is not reproduced in experiment 3/3 performed in the same bicarbonate concentration.

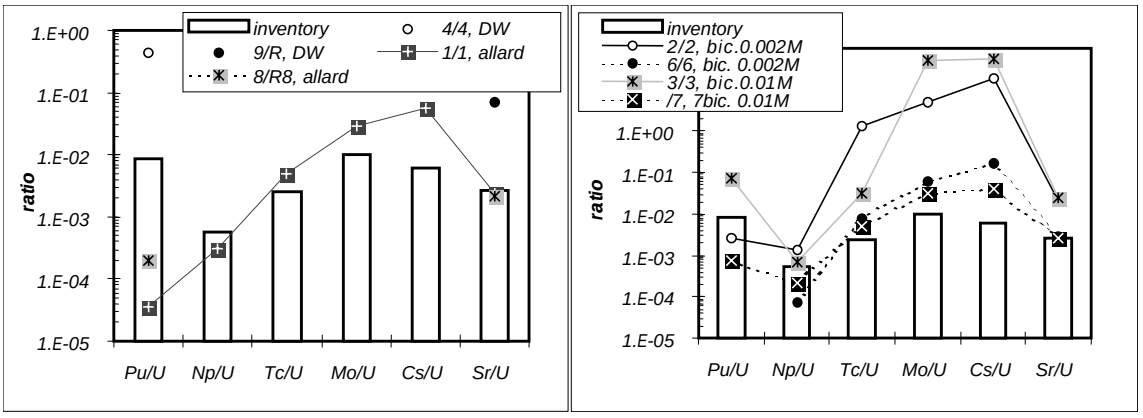

Figure 5-28. *Radionuclide to uranium ratios in versus their ratio according to inventory.*

Concerning technetium and molybdenum, the corresponding ratios calculated in solution with respect the uranium are slightly over the inventory ratio, particularly for Mo. This fact can be explained by similar reasoning as in the time resolved experiments. Experiment 2/2 shows a suspicious enrichment for all radionuclides determined in solution, as compared to their inventory ratios. The results from this experiment should be taken with some caution.

Caesium to uranium ratios in solution are larger than the inventory ratio as expected according to the reasoning used in the time-resolved experiments.

Finally strontium to uranium ratios are, as expected, quite close to the inventory ratio in all the tests with the exception of the experiment performed in distilled water. This unusual behaviour could be the result of the precipitation of U(VI) in the form of schoepite, resulting in an enrichment of Sr with respect to U in solution.

As in the case of the time-resolved experiments, we have estimated the redox potential of the experimental systems, prior to the equilibrium modelling. The pe has been calculated assuming equilibrium between the redox couples considered in equations 5-5 to 5-10. In the case of the uranium system, due to the varying chemical conditions, the predominant equilibrium changes as a function of the bicarbonate concentration.

The apparent lack of consistency between the calculated pe based on the radiolytic products and the values based do not give much confidence in the estimated values (see Figure 5-29). However, these calculations would indicate that the system remains slightly reducing, particularly in bicarbonate media. As a first approximation we will use the pe calculated from the UO_2/U(VI) pair in order to establish the potential saturation state of the experimental solutions with respect to radionuclide solid phases.

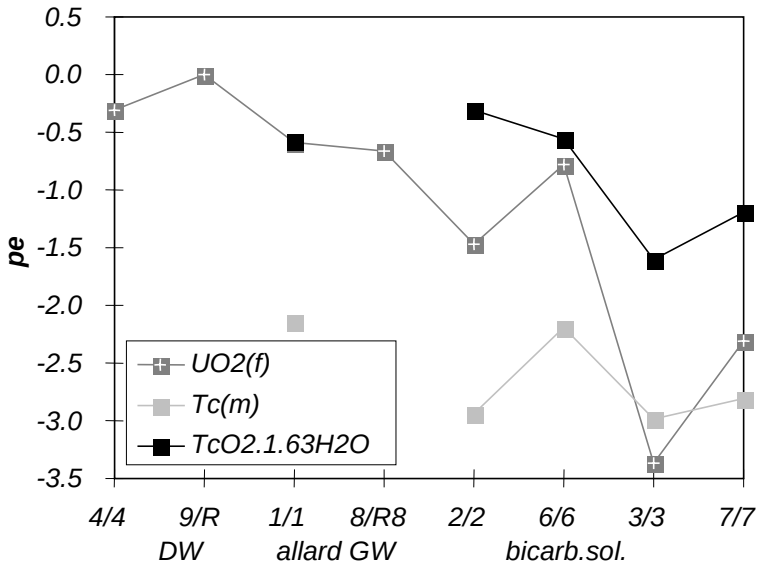

Figure 5-29. *Calculated pe assuming the different redox couples (see text).*

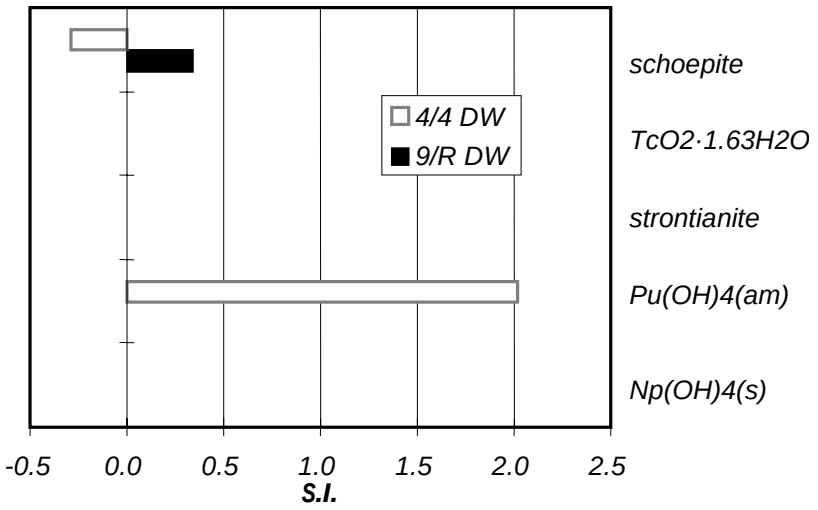

Figure 5-30. *Saturation indexes of the most favoured solid phases in the experiments performed by using distilled water as leaching solution.*

The results of these calculations are given in the next figures (Figures 5-30 to 5-33).

Uranium appears to be in equilibrium with schoepite in the experiments performed in deionised water. Pu appears to be oversaturated with respect to $Pu(OH)_4(s)$ in these experiments. Strontium is not limited by any pure solid phase which is in agreement with the discussions in the previous section.

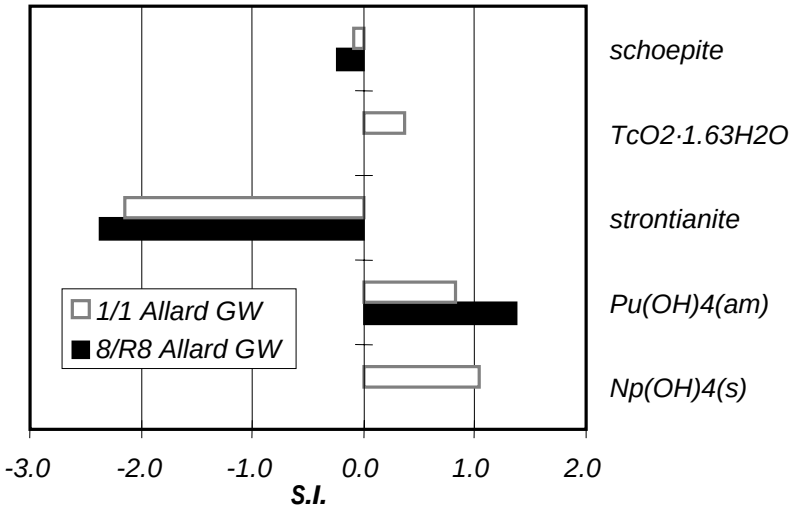

Figure 5-31. *Saturation indexes of the most favoured solid phases in the experiments performed by using Allard synthetic groundwater*

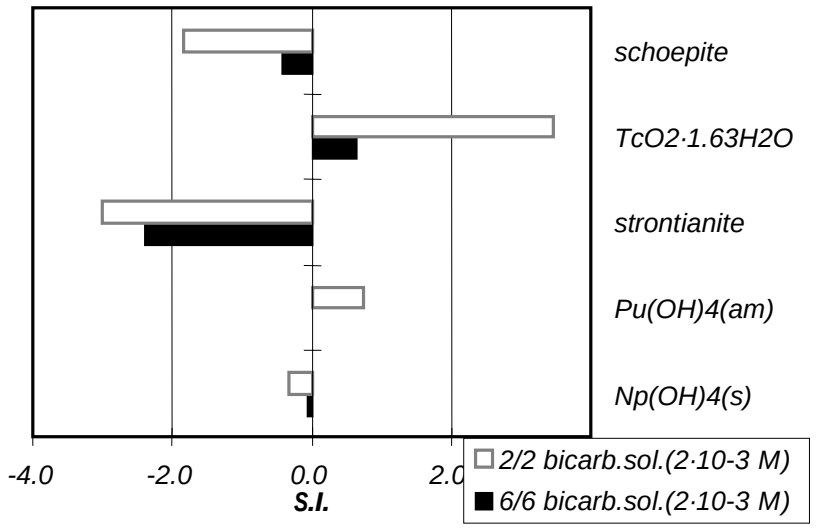

Figure 5-32. *Saturation indexes of the most favoured solid phases in the experiments performed by using the bicarbonate solution ($2 \cdot 10^{-3}$ mole·dm^{-3}) as leaching solution.*

As in the previous experiments, uranium appears to be in equilibrium with schoepite in the experiments performed in 2 millimolar bicarbonate concentration (either as Allard groundwater or in plain bicarbonate solution). Sr is undersaturated with respect to strontianite in these experiments. Hence, as in the previous case, the concentration of this metal in solution is expected to be limited by a co-dissolution process with the major component of the fuel matrix. Plutonium and neptunium appear in general close to saturation with respect the most favoured pure solid phases under these experimental conditions, their tetravalent hydroxide. Finally, Tc release under these conditions appears to be controlled by the solubility of Tc(IV) hydroxide.

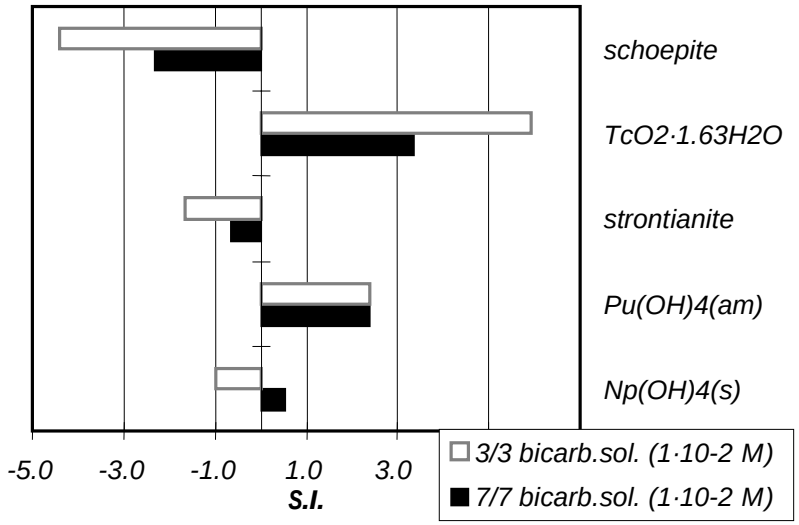

Figure 5-33. *Saturation indexes of the most favoured solid phases in the experiments performed by using the bicarbonate solution (10^{-2} mole·dm^{-3}) as leaching solution.*

At the highest bicarbonate concentration, uranium is undersaturated with respect to schoepite. Hence, no secondary phase formation appears to control the uranium release. Strontianite is slightly under-saturated and consequently the same reasoning as in the previous tests can be applied. The saturation indexes obtained for Np and Pu indicate that, as in the previous experiments, their concentrations in solution are limited by the precipitation of secondary pure solid phases. Finally, the release of technetium appears to be controlled by the secondary precipitation of Tc(IV) hydroxide.

6 Conclusions

The present work reported indicates that carefully controlled mass balance radiolytic experiments are useful to ascertain the mechanisms responsible for spent fuel stability and radionuclide release under repository conditions. In this context, the time-resolved experiments have proven to be particularly suitable to gain a mechanistic insight on the key processes related to water radiolysis, matrix oxidation and radionuclide dissolution.

Concerning the production and fate of radiolytic products at the spent fuel/water interface, the present experimental data and the electron mass balance calculations analysis indicate that the excess of oxidants produced is readily scavenged by the reducing capacity of the uranium(IV) dioxide fuel matrix. The main oxidant scavenging processes are either the formation of an oxidised UO_{2+x} surface layer in deionised water, and/or the formation of soluble U(VI)-carbonate species in bicarbonate media. The formation of the oxidised surface layer has a relevant impact on the decomposition of H_2O_2 and the formation of secondary radiolytic products. The presence of chloride ions seems to have an important effect on the oxidant generation by radiolytic water decomposition.

The analysis of the redox dependent components, as determined from the time-resolved experiments, indicate that a redox equilibrium situation is established between the dissolved radiolytic products (H_2, O_2 and H_2O_2), the UO_2/U(VI) and the Tc(m)/TcO_4^- redox pairs. The resulting pe in the bulk solution is in the range –3.0 to –2.6. This could indicate that reducing conditions are restored in the aqueous phase at sufficient distance away from the dynamic redox spent fuel/water interface. Actual redox measurements in these time-resolved experiments should be useful to validate or falsify this hypothesis.

The analysis of the redox data from the long time experiments is less conclusive. However, the data concerning the U and Tc redox pairs could indicate that the bulk solution remains slightly reducing, even when the oxidative alteration of the fuel matrix has proceeded up to U(VI) oxyhydroxide formation. Again, actual redox measurements during the experiments are critical to ascertain the validity of this hypothesis.

Concerning the radionuclide dissolution data, the present experiments have helped to confirm in a more mechanistic manner some of the observations already made from the very long term spent fuel leaching experiments. Uranium dissolution at the early contact times is controlled by the oxidative oxidation of the UO_2 matrix . This process controls the co-dissolution of most of the measured radionuclides, Sr, Np and Pu. Although the solubility of the actinides appear to be limited by the formation of Ac(IV) hydroxide phases. This is particularly noticeable in the case of Pu. Sr-90 shows no solubility control during the whole series of experiments which would confirm the reliability of this nuclide as matrix alteration marker. The release of Tc and Mo appears to be controlled by the oxidative dissolution of their metallic phases, with Mo showing a higher oxygen affinity than Tc in agreement with their relative thermodynamic properties. The behaviour of the lanthanide elements (Nd and Y) is quite surprising and does not shown any indication of congruent release with the fuel matrix. Cs behaves as expected with a preferential dissolution pattern in agreement with previous observations.

The storage conditions of the spent fuel fragments seem to have a marked effect on the radiolytic product generation and consequently on the radionuclide release. The experiments performed with untreated spent fuel fragments which have been stored in air indicate the existence of an oxidised UO_{2+x} surface layer. This oxidised surface layer contains an enriched content of minor radionuclides which result in an enhanced release of all the measured radionuclides Pu, Np, Tc, Mo, La, Y, Sr and Cs. This effect disappears once the surface of the spent fuel fragments has been renewed.

The longer contact time experiments indicate that after the initial oxidative dissolution process some of the elements reach saturation with respect to secondary phases. Uranium concentrations seem to be in equilibrium with U(VI)-oxyhydroxide in all the experiments, except for the ones performed in the largest bicarbonate concentration (10 mM). In this case the stability of the U(VI) carbonate complexes hinders the precipitation of any secondary phase. Pu and Np seem to be solubility limited by the formation of their Ac(IV) hydroxide phases. The oxidative dissolution of Tc seems also to be controlled by the formation of a secondary Tc(IV) hydroxide phase. Sr is not close to equilibrium with any secondary phase confirming its role as matrix dissolution marker.

Future work in this area should concentrate on establishing the mechanism and rates of radiolytic product generation and fate by dedicated experiments. Furthermore, the role of carbonate and chloride in the generation of radiolytic products should be explored and quantified. Additionally, some of the hypothesis pointed out in this work by the thermodynamic calculations should be verified by appropriate measurements, in particular the redox condition of the bulk solution and the potential secondary phase formation. We feel that the experimental methodology presented in this work will continue to help us to gain the required mechanistic insight on these critical processes for spent fuel stability under repository conditions.

7 References

Bruno J, Cera E, Duro L, Ahonen L, 1996. Deep groundwater redox reactions in the Palmottu uranium deposit: The role of uranium and iron in these processes. POSIVA-96-24.

Bruno J, Cera E, Duro L, Pon J, de Pablo J, Eriksen T E, 1998. Development of a kinetic model for the dissolution of the UO_2 spent nuclear fuel. Application of the model to the minor radionuclides. SKB TR 98-22, Svensk Kärnbränslehantering AB.

Casas I, Bruno J, 1994. What have we learned about Spent Fuel Dissolution in Cigar Lake? Within the Final Report of the AECL/SKB Cigar Lake Analog Study. SKB TR 94-04, Svensk Kärnbränslehantering AB.

Eriksen T E, Eklund U-B, Werme L O, Bruno J, 1995. Dissolution of irradiated fuel: a radiolytic mass balance study. J. Nucl. Mater. 227, 76–82.

Forsyth R, 1995. Spent nuclear fuel. A review of properties of possible relevance to corrosion processes. SKB TR 95-23, Svensk Kärnbränslehantering AB.

Forsyth R, 1997. The SKB spent fuel corrosion programme. An evaluation of results from the experimental programme performed in the Studsvik hot cell laboratory. SKB TR 97-25, Svensk Kärnbränslehantering AB.

Forsyth R, Eklund U-B, Mattson O, Schrire D, 1990. Examination of the surface deposit on an irradiated PWR fuel specimen subjected to corrosion in deionised water. SKB TR 90-04, Svensk Kärnbränslehantering AB.

Forsyth R S, Werme L O, 1991. Spent fuel corrosion and dissolution. SKB TR 91-60, Svensk Kärnbränslehantering AB.

Forsyth R S, Werme L O, 1992. Spent fuel corrosion and dissolution. J. Nucl. Mater. 190, 3–19.

Gray W J, 1998. Spent fuel dissolution rates as a function of burnup and water chemistry. PNNL-11895.

Hanson B D, 1998. The burnup dependence of light water reactor spent fuel oxidation. PNNL-11929.

Kleykamp H, 1988. The chemical state of fission products in oxide fuels at different stages of the nuclear fuel cycle. Nuclear Technology, 80, 412–422.

Stumm W, Morgan J J, 1981. Aquatic chemistry. John Wiley and Sons, 2ond ed.

White A F, Yee A, 1985. Aqueous oxidation-reduction kinetics associated with coupled electron-cation transfer from iron-containing silicates at 25°C. Geochim. et Cosmochim. Acta, 49, 1263–1275.

Table 8-1. Hydrogen, oxygen and hydrogen peroxide concentrations, generated by water radiolysis.

	Contact time hours	Vgas cc	H_2 ppm	O_2 ppm	Contact time hours	Vsol ml	pH	H_2O_2 mole·dm^{-3}
7:40:1:I	0	30	53	43	1.33	30	8.75	
7:40:1:II	18.75	30.75	110	128	26.33	29.25	8.87	$2.50 \cdot 10^{-8}$
7:40:1:III	41.5	32.85	248	176	46.5	27.15	8.88	$3.80 \cdot 10^{-8}$
7:40:1:IV	67.75	35.13	426	214	68.5	24.87	8.98	$4.30 \cdot 10^{-8}$
7:40:1:V	116	36.85	674	276	117.5	23.15	8.96	$7.30 \cdot 10^{-8}$
7:40:1:VI	164	39.21	797	322	166	20.79	8.82	$8.50 \cdot 10^{-8}$
7:40:1:VII	308	41.56	898	439	312.5	18.44	8.80	$1.20 \cdot 10^{-7}$
7:40:2:0	3.5	30	123	13				
7:40:2:I	47.25	30	466	44.0	51.25	30	8.99	$8.10 \cdot 10^{-7}$
7:40:2:II	119.3	32.29	865	96.0	122	28.29	8.98	$4.80 \cdot 10^{-7}$
7:40:2:III	191.3	34.59	1102	160.0	194.8	26.57	8.99	$3.10 \cdot 10^{-7}$
7:40:2:IV	287.5	37.25	1185	236.0	290.25	24.28	9.12	$2.60 \cdot 10^{-7}$
7:40:2:V	359.5	39.4	1232	287.0	361	22.9	9.18	$2.40 \cdot 10^{-7}$
7:40:2:VI	1033	41.68			1033	18.32		
7:40:3:I	0.33	30	45	15	0.5	30	8.86	
7:40:3:II	68	31.73	360	133	70	28.27	9.02	$8.00 \cdot 10^{-7}$
7:40:3:III	140	34.3	668	214	142	25.7	9.10	$5.30 \cdot 10^{-7}$
7:40:3:IV	235.6	36.81	969	302	236	23.19	8.97	$3.80 \cdot 10^{-7}$
7:40:3:V	284	39.79	1085	360	285	20.22	8.98	$3.60 \cdot 10^{-7}$
7:40:3:VI	907	42.82	4031	1076	907	17.18	8.78	$1.50 \cdot 10^{-7}$
7:40:4:I	169.5	30	797	288	170	30	8.85	$1.04 \cdot 10^{-6}$
7:40:4:II	384.5	33.7	1439	382	387	26.3	8.90	$3.20 \cdot 10^{-7}$
7:40:4:III	551.8	37.2	2004	364	555	22.8	9.05	$2.10 \cdot 10^{-7}$
7:40:4:IV	649.2	40.7	2051	383	653	19.3	9.05	$1.65 \cdot 10^{-7}$

Table 8-2. Radionuclide concentrations determined in solution.

	Time hours	Y	Mo	Cs	Tc	Nd	Np	Pu	U	Sr
						mole·dm^{-3}				
7:40:1:I	1.3	$2.16\cdot10^{-8}$	$3.93\cdot10^{-7}$	$2.23\cdot10^{-7}$	$4.18\cdot10^{-8}$	$5.85\cdot10^{-8}$	$8.10\cdot10^{-9}$	$6.42\cdot10^{-8}$	$2.89\cdot10^{-5}$	$4.82\cdot10^{-8}$
7:40:1:II	26	$1.97\cdot10^{-8}$	$6.30\cdot10^{-7}$	$7.87\cdot10^{-7}$	$5.56\cdot10^{-8}$	$6.30\cdot10^{-8}$	$5.48\cdot10^{-9}$	$6.50\cdot10^{-8}$	$5.35\cdot10^{-5}$	$8.12\cdot10^{-8}$
7:40:1:III	47	$2.19\cdot10^{-8}$	$8.37\cdot10^{-7}$	$1.53\cdot10^{-6}$	$8.01\cdot10^{-8}$	$5.73\cdot10^{-8}$	$8.88\cdot10^{-9}$	$6.38\cdot10^{-8}$	$6.46\cdot10^{-5}$	$1.09\cdot10^{-7}$
7:40:1:IV	69	$2.31\cdot10^{-8}$	$9.92\cdot10^{-7}$	$1.76\cdot10^{-6}$	$1.13\cdot10^{-7}$	$6.10\cdot10^{-8}$	$9.33\cdot10^{-9}$	$8.39\cdot10^{-8}$	$6.79\cdot10^{-5}$	$1.22\cdot10^{-7}$
7:40:1:V	118	$4.31\cdot10^{-8}$	$1.37\cdot10^{-6}$	$2.45\cdot10^{-6}$	$1.78\cdot10^{-7}$	$8.40\cdot10^{-8}$	$1.09\cdot10^{-8}$	$1.06\cdot10^{-7}$	$7.62\cdot10^{-5}$	$1.89\cdot10^{-7}$
7:40:1:VI	166	$3.31\cdot10^{-8}$	$1.60\cdot10^{-6}$	$3.33\cdot10^{-6}$	$2.24\cdot10^{-7}$	$8.41\cdot10^{-8}$	$1.02\cdot10^{-8}$	$1.05\cdot10^{-7}$	$1.04\cdot10^{-4}$	$1.98\cdot10^{-7}$
7:40:1:VII	313	$2.75\cdot10^{-8}$	$2.33\cdot10^{-6}$	$4.42\cdot10^{-6}$	$3.68\cdot10^{-7}$	$7.77\cdot10^{-8}$	$1.57\cdot10^{-8}$	$1.18\cdot10^{-7}$	$1.58\cdot10^{-4}$	$2.67\cdot10^{-7}$
7:40:2:I	51	$5.55\cdot10^{-9}$	$3.00\cdot10^{-7}$	$7.49\cdot10^{-7}$	$5.47\cdot10^{-8}$	$8.10\cdot10^{-9}$	$4.08\cdot10^{-9}$	$1.09\cdot10^{-8}$	$2.14\cdot10^{-5}$	$5.60\cdot10^{-8}$
7:40:2:II	122	$1.09\cdot10^{-8}$	$3.80\cdot10^{-7}$	$9.60\cdot10^{-7}$	$9.53\cdot10^{-8}$	$1.91\cdot10^{-8}$	$6.73\cdot10^{-9}$	$1.01\cdot10^{-8}$	$2.91\cdot10^{-5}$	$6.48\cdot10^{-8}$
7:40:2:III	195	$3.93\cdot10^{-9}$	$6.19\cdot10^{-7}$	$1.19\cdot10^{-6}$	$8.31\cdot10^{-8}$	$1.34\cdot10^{-9}$	$6.08\cdot10^{-9}$	$3.52\cdot10^{-9}$	$2.47\cdot10^{-5}$	$8.06\cdot10^{-8}$
7:40:2:IV	290	$3.71\cdot10^{-9}$	$8.61\cdot10^{-7}$	$1.73\cdot10^{-6}$	$1.39\cdot10^{-7}$	$2.55\cdot10^{-9}$	$5.91\cdot10^{-9}$	$3.64\cdot10^{-9}$	$4.55\cdot10^{-5}$	$1.07\cdot10^{-7}$
7:40:2:V	361	$3.67\cdot10^{-9}$	$9.83\cdot10^{-7}$	$1.98\cdot10^{-6}$	$1.42\cdot10^{-7}$	$2.26\cdot10^{-9}$	$8.25\cdot10^{-9}$	$2.57\cdot10^{-9}$	$5.37\cdot10^{-5}$	$1.08\cdot10^{-7}$
7:40:2:VI	1033		$1.54\cdot10^{-6}$	$2.67\cdot10^{-6}$	$4.31\cdot10^{-7}$	$2.60\cdot10^{-8}$	$1.40\cdot10^{-8}$	$2.45\cdot10^{-8}$	$8.30\cdot10^{-5}$	$1.68\cdot10^{-6}$
7:40:3:I	0.5	$4.57\cdot10^{-9}$	$1.24\cdot10^{-7}$	$1.45\cdot10^{-7}$	$2.45\cdot10^{-8}$	$4.38\cdot10^{-9}$	$1.30\cdot10^{-9}$	$6.49\cdot10^{-9}$	$5.45\cdot10^{-6}$	$2.77\cdot10^{-8}$
7:40:3:II	70	$4.62\cdot10^{-9}$	$1.91\cdot10^{-7}$	$1.88\cdot10^{-7}$	$4.36\cdot10^{-8}$	$5.06\cdot10^{-9}$	$3.88\cdot10^{-9}$	$6.63\cdot10^{-9}$	$8.14\cdot10^{-6}$	$3.85\cdot10^{-8}$
7:40:3:III	142	$5.54\cdot10^{-9}$	$2.99\cdot10^{-7}$	$2.65\cdot10^{-7}$	$6.53\cdot10^{-8}$	$4.10\cdot10^{-9}$	$4.89\cdot10^{-9}$	$3.79\cdot10^{-9}$	$1.51\cdot10^{-5}$	$4.17\cdot10^{-8}$
7:40:3:IV	236	$3.80\cdot10^{-9}$	$4.56\cdot10^{-7}$	$3.91\cdot10^{-7}$	$1.04\cdot10^{-7}$	$3.32\cdot10^{-9}$	$6.50\cdot10^{-9}$	$3.57\cdot10^{-9}$	$2.58\cdot10^{-5}$	$4.95\cdot10^{-8}$
7:40:3:V	285	$6.77\cdot10^{-9}$	$6.48\cdot10^{-7}$	$5.75\cdot10^{-7}$	$1.49\cdot10^{-7}$	$4.58\cdot10^{-9}$	$8.67\cdot10^{-9}$	$3.78\cdot10^{-9}$	$3.35\cdot10^{-5}$	$7.64\cdot10^{-8}$
7:40:3:VI	907	$3.51\cdot10^{-9}$	$1.28\cdot10^{-6}$	$1.05\cdot10^{-6}$	$3.64\cdot10^{-7}$	$5.12\cdot10^{-9}$	$1.93\cdot10^{-8}$	$1.52\cdot10^{-9}$	$1.02\cdot10^{-4}$	$1.35\cdot10^{-7}$
7:40:4:I	170	$6.97\cdot10^{-9}$	$2.70\cdot10^{-7}$	$4.52\cdot10^{-7}$	$6.67\cdot10^{-8}$	$4.03\cdot10^{-9}$	$6.41\cdot10^{-9}$	$2.75\cdot10^{-9}$	$1.21\cdot10^{-5}$	$7.69\cdot10^{-8}$
7:40:4:II	387	$3.93\cdot10^{-9}$	$6.05\cdot10^{-7}$	$4.52\cdot10^{-7}$	$1.53\cdot10^{-7}$	$2.08\cdot10^{-9}$	$1.08\cdot10^{-8}$	$2.96\cdot10^{-9}$	$2.55\cdot10^{-5}$	$8.07\cdot10^{-8}$
7:40:4:III	555	$3.82\cdot10^{-9}$	$7.59\cdot10^{-7}$	$5.78\cdot10^{-7}$	$1.72\cdot10^{-7}$	$2.85\cdot10^{-9}$	$1.27\cdot10^{-8}$	$2.92\cdot10^{-9}$	$3.59\cdot10^{-5}$	$1.01\cdot10^{-7}$
7:40:4:IV	653	$4.38\cdot10^{-9}$	$1.24\cdot10^{-6}$	$7.85\cdot10^{-7}$	$2.68\cdot10^{-7}$	$2.43\cdot10^{-9}$	$1.51\cdot10^{-8}$	$3.08\cdot10^{-9}$	$4.04\cdot10^{-5}$	$1.16\cdot10^{-7}$

Table 8-3. Radiolysis products and radionuclide concentrations determined in the long time experiments.

Radiolysis products							
reference	**solution**	**$[C]_{tot}$**	**contact time**	**pH**	**O_2(g)**	**H_2(g)**	**H_2O_2**
		mole·dm^{-3}	**days**		**% Vol**	**% Vol**	**moles**
4/4	dw	0	372	7.90	2.80	6.30	$1.45 \cdot 10^{-5}$
9/R	dw	0	460	7.92	3.80	9.50	$3.50 \cdot 10^{-6}$
1/1	allard GW	$2.01 \cdot 10^{-3}$	396	8.28	3.00	3.30	$5.00 \cdot 10^{-8}$
8/R8	allard GW	$2.01 \cdot 10^{-3}$	417	8.28	2.50	5.00	$1.00 \cdot 10^{-7}$
2/2	bicarb. sol.	$2.00 \cdot 10^{-3}$	390	8.30	0.90	2.80	$6.10 \cdot 10^{-6}$
6/6	bicarb. sol.	$2.00 \cdot 10^{-3}$	463	8.30	1.40	3.60	$1.10 \cdot 10^{-6}$
3/3	bicarb. sol.	$1.00 \cdot 10^{-2}$	392	8.90	0.03	5.60	$8.00 \cdot 10^{-8}$
7/7	bicarb. sol.	$1.00 \cdot 10^{-2}$	455	8.90	1.40	2.90	$2.00 \cdot 10^{-7}$

Radionuclide concentrations							
reference	**U**	**Pu**	**Np**	**Tc**	**Mo**	**Cs**	**Sr**
				mole·dm^{-3}			
4/4	$2.10 \cdot 10^{-7}$	$9.26 \cdot 10^{-8}$					
9/R	$1.05 \cdot 10^{-6}$						$7.41 \cdot 10^{-8}$
1/1	$1.60 \cdot 10^{-4}$	$5.85 \cdot 10^{-9}$	$5.06 \cdot 10^{-8}$	$7.78 \cdot 10^{-7}$	$4.69 \cdot 10^{-6}$	$8.91 \cdot 10^{-6}$	$3.89 \cdot 10^{-7}$
8/R8	$1.05 \cdot 10^{-4}$	$2.09 \cdot 10^{-8}$					$2.22 \cdot 10^{-7}$
2/2	$1.85 \cdot 10^{-6}$	$4.89 \cdot 10^{-9}$	$2.41 \cdot 10^{-9}$	$2.43 \cdot 10^{-6}$	$9.66 \cdot 10^{-6}$	$3.41 \cdot 10^{-5}$	$3.70 \cdot 10^{-8}$
6/6	$5.88 \cdot 10^{-5}$		$4.22 \cdot 10^{-9}$	$4.44 \cdot 10^{-7}$	$3.58 \cdot 10^{-6}$	$9.92 \cdot 10^{-6}$	$1.67 \cdot 10^{-7}$
3/3	$2.94 \cdot 10^{-6}$	$2.19 \cdot 10^{-7}$	$2.11 \cdot 10^{-9}$	$9.19 \cdot 10^{-8}$	$1.46 \cdot 10^{-4}$	$1.62 \cdot 10^{-4}$	$7.41 \cdot 10^{-8}$
7/7	$3.11 \cdot 10^{-4}$	$2.26 \cdot 10^{-7}$	$6.75 \cdot 10^{-8}$	$1.58 \cdot 10^{-6}$	$9.91 \cdot 10^{-6}$	$1.26 \cdot 10^{-5}$	$7.96 \cdot 10^{-7}$